Additive Manufacturing as a Method to Design and Optimize Bioinspired Structures

Audrey Velasco-Hogan, Jun Xu, and Marc A. Meyers*

Additive manufacturing (AM) is a current technology undergoing rapid development that is utilized in a wide variety of applications. In the field of biological and bioinspired materials, additive manufacturing is being used to generate intricate prototypes to expand our understanding of the fundamental structure–property relationships that govern nature's spectacular mechanical performance. Herein, recent advances in the use of AM for improving the understanding of the structure–property relationship in biological materials and for the production of bioinspired materials are reviewed. There are four essential components to this work: a) extracting defining characteristics of biological designs, b) designing 3D-printed prototypes, c) performing mechanical testing on 3D-printed prototypes to understand fundamental mechanisms at hand, and d) optimizing design for tailorable performance. It is intended to highlight how the various types of additive manufacturing methods are utilized, to unravel novel discoveries in the field of biological materials. Since AM processing techniques have surpassed antiquated limitations, especially with respect to spatial scales, there has been a surge in their demand as an integral tool for research. In conclusion, current challenges and the technical perspective for further development of bioinspired materials using AM are discussed.

1. Introduction

The field of biological materials, representing the entrance of materials science and engineering into biology, is rapidly advancing.[1–4] The characterization, analysis, and computational tools of materials science are being implemented in biology to elucidate numerous phenomena and effects from an engineering perspective. The structure–property–performance approach traditionally applied to metallic, ceramic, polymeric, and composite materials is now being applied to materials found in nature. The emerging field of bioinspiration is defined by the translation of materials science and engineering

principles to biological materials and synthetic designs. Here, we focus on how additive manufacturing (AM) is used to generate bioinspired structures and the subsequent lessons learned. The ability for AM to readily manufacture intricate structures grants considerable access to explore the structure–property relationships in biological materials. Therefore, the inherent features and fundamental design motifs of biological materials is discussed in this section. We conclude with the current challenges of AM which include multiscalability, multimaterial interfaces, and the control of inherent defects. We propose that the future direction of the field of bioinspired design will rely on advances in multiprocess 3D printing and analytical techniques to better understand the fundamental behavior of biological materials.

At least seven unique aspects of biological materials distinguish them from their synthetic counterparts. It is through the understanding of each of them that we are advancing our knowledge, with the goal of generating novel bioinspired materials and designs. These defining aspects comprise the Arzt heptahedron,[5,6] presented in **Figure 1**. They are as follows:

- *Self-Organization*: Nature synthesizes materials via a bottom-up[7] approach, which involves the self-assembly of precursors to generate a predetermined structure. In contrast, many traditional manufacturing processing methods use the top-down approach, which is defined by bulk processing, in which the larger features of the material are reduced to generate the desired form, making it difficult to control the nanoscale features. The bottom-up approach used by nature engenders self-organization and self-assembly all the way from the nanoscale to the macroscale.

- *Self-Healing*: Many biological materials have a self-healing capability enabled by the cells and vascularity embedded in the extracellular matrix. These cells act as "diffuse command centers" in the biological materials and enlist the mechanism of healing. Only a minute number of synthetic materials have this capability.

- *Evolution and Environmental Constraints*: Whereas the history of development of synthetic materials is, at the most, a few thousand years old, and in many cases, hundred years or less, biological materials have evolved for three billion years.

A. Velasco-Hogan, M. A. Meyers
University of California
San Diego, La Jolla, CA 92093, USA
E-mail: mameyers@eng.ucsd.edu
J. Xu
Department of Automotive Engineering
School of Transportation Science and Engineering
Advanced Vehicle Research Center (AVRC)
Beihang University
Beijing 100191, China
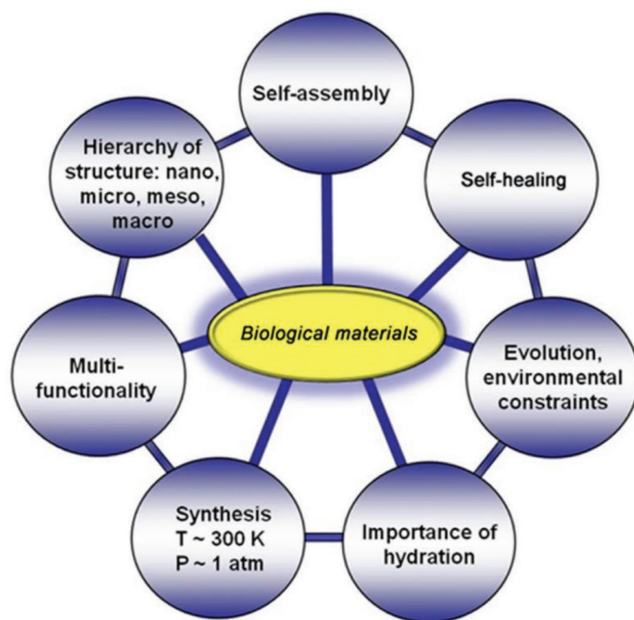
Figure 1. Seven unique characteristics of biological materials: the Arzt heptahedron. Adapted with permission.[5] Copyright 2006, Elsevier.

Marc A. Meyers is a distinguished professor of Materials Science at the University of California, San Diego. His research field is the mechanical behavior of materials with a focus on three areas: dynamic behavior of materials, nanocrystalline materials, and biological materials. He was a cofounder of the Center for Explosives Technology Research, New Mexico Tech, and the EXPLOMET conference series, as well as Associate Director and Director of the UCSD Institute for Mechanics and Materials.

These biological materials developed through a process of evolution, driven by natural selection.

- *Importance of Hydration*: With notable exceptions, such as enamel and a few minerals, the level of hydration determines the mechanical properties. There are dramatic changes when biological materials are dehydrated.

- *Synthesis at ambient Temperature and Pressure*: Nature does not utilize furnaces for high-temperature reactions or autoclaves for high-pressure processing of materials. Nor does she need them since organisms exist mostly in a narrow range (−50 to +50 °C) of temperatures. There are isolated cases such as extremophiles and organisms living close to deep-sea vents, but they represent the exception. On the other hand, synthetic materials are designed to resist a variety of environments such as high temperatures and pressures.

- *Multifunctionality*: Many tissues have more than one function, and this provides economy of space and mass. For example, the arthropod exoskeleton provides structural support for the body, protection from predators, serves as an attachment to the muscles, and controls the exchange with fluids with the surroundings, and is able to resist mechanical loads.[8] Since the exoskeleton can perform all of these functions, arthropods can conserve the need for additional specialized tissues.

- *Hierarchy of Structure*: This is an aspect of utmost importance because it has direct relevance to the material's mechanical properties. The structures at the nano-, micro-, meso-, and ultralevels have different characteristics and work together synergistically. For example, the hierarchical structure of bone, which has been described in numerous reviews,[9–11] relies on the varying mechanical properties at different structural levels to mitigate crack propagation and enhance toughness. Collagen fibers and hydroxyapatite minerals are organized at the nanoscale to effectively build the microscale features consisting of lamellar sheets wrapped in concentric layers. The

microstructure ultimately forms the macrostructure, defined as either cortical or cancellous bone. This is not an obvious strategy implemented in the design of engineered materials.

These unique characteristics render biological materials intrinsically different from synthetic materials.

Although there is a daunting variety of organisms (≈8 million species), there are a few recurring motifs in biological materials. They were identified, for the first time, by Naleway et al.[12] using an approach introduced by Meyers et al.[2] This consists of seeking common structural designs in biological materials. They are collectively named "structural design elements" and are amenable to analytical treatment. They occur in different species through convergence and parallelism processes. Eight structural design elements are shown in **Figure 2** and they are briefly described below:

- *Fibrous Structures*: These have high tensile strength when aligned in a single direction, and undergo buckling readily under compression resulting in low compressive strength.

- *Helical/Bouligand Structures*: Common to fibrous or composite materials, these are characterized by the rotation of the fibers in sequential layers. Enhanced toughness results from the difficulty in propagating cracks; in-plane isotropy of strength and stiffness can be achieved with fibers.

- *Gradient Structures*: Materials and interfaces that accommodate property mismatch (e.g., elastic modulus) through a gradual transition. This design aids in increasing toughness by avoiding the buildup of interfacial mismatch stress.

- *Composite/Layered Structures*: Complex composites that increase the toughness of (most commonly) brittle materials through the introduction of interfaces. A classic example is the nacreous structure in shells, such as abalone.

- *Tubular Structures*: Organized porosity that enables energy absorption and crack deflection.

- *Cellular Structures*: Lightweight porous or foam architectures that provide directed stress distribution and energy absorption.

- *Suture Interfaces*: Compliant interlocking seams that connect stiffer components.

**ADVANCED
SCIENCE NEWS**

www.advancedsciencenews.com

**ADVANCED
MATERIALS**

www.advmat.de
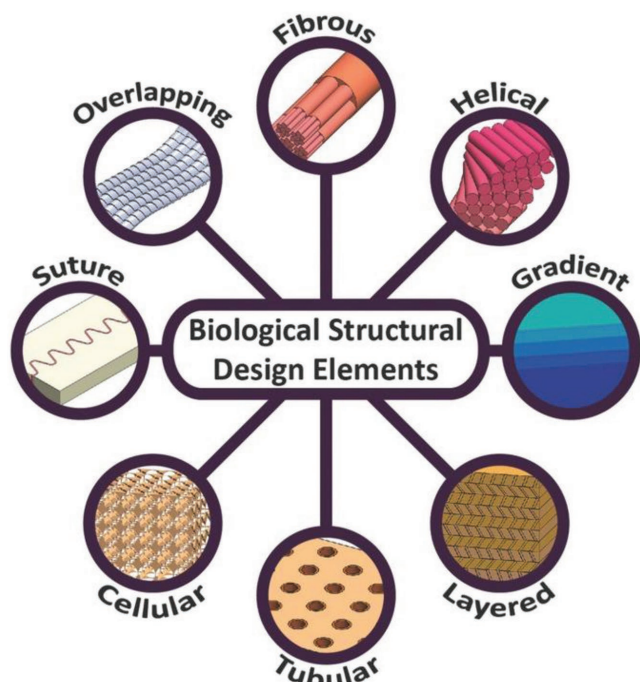
Figure 2. The eight principal structural design elements: motifs that appear in different species through the processes of convergent evolution and parallelism. Reproduced with permission.[12] Copyright 2015, Wiley-VCH.

- *Articulated Structures*: Overlapping plates that slide past each other to make a rigid yet flexible surface suitable for armor. Primary examples are fish and pangolin scales and the tail of the seahorse.

Here, we use the above defining aspects and structural design elements of biological materials to lay the framework for the studies highlighted in Section 3. Each of the studies described is classified within the following categories: composite/layered,

hierarchical, suture, articulated, helical, cellular, and shape-morphing structures; and structured surfaces. Within each category the methods and analyses of bioinspired AM models are discussed.

The structural architecture of biological materials is essentially based on two elements: an organic and a mineral component. Minerals provide compressive strength and stiffness, whereas the organic (biopolymer) component provides tensile strength. The ingenious manner by which these biocomposite structures are engineered is responsible for a superior mechanical response when compared to their synthetic counterparts. **Figure 3**, first introduced by Ashby et al.[13] and then modified by Fratzl et al.,[11] Espinosa et al.,[14] and Zavattieri and co-workers,[15] illustrates the relationship between two important mechanical performance parameters, the toughness (ability to resist fracture) and stiffness (ability to resist elastic deformation). In synthetic materials, the increase in elastic modulus is associated with a decrease in toughness; metals (with a lower elastic modulus) are tougher than ceramics. This dependence is strong and it has not been possible to produce ceramics with high toughness[13,16] despite a sustained research effort over one century. For biological materials, the ingenious multiscale and hierarchical mixing of the inorganic and organic components leads to an inverse response when compared to synthetic materials. The sensitivity to stiffness is much lower and the stiffness can be considerably increased without a decrease in toughness up to a critical value. The performance space is significantly enhanced for biological materials, which have unique architectures for toughness enhancement. This is an important difference, one that materials designers would love to emulate.

The creation of bioinspired designs has been limited by the ability to synthesize and assemble materials with different hierarchical levels using traditional manufacturing methods. With recent advancements in AM, which utilizes a bottom-up approach analogous to nature, this limitation has been resolved. Materials found in nature are synthesized via a bottom-up approach where their final structure is encoded in their precursors that self-assemble to the prescribed form. The assembly of building blocks across multiple length scales leads to the generation of hierarchical structures. On the contrary, traditional manufacturing processes use the top-down approach, where the desired material is formed from the reduction of the bulk material or by bulk solidification. This method, beginning with the bulk material, makes it difficult to generate hierarchies across many length scales. While many bottom-up manufacturing processes exist, such as physical vapor deposition (PVD), chemical vapor deposition (CVD), and sputtering, they have severe size and thickness limitations and do not lend themselves well to the scale-up requirements of structural materials. AM has been the focus of significant research effort in recent years as it uses a bottom-up approach and can be scaled up. Although AM is not currently ideal for producing a large quantity of items at once, it opens a plethora of opportunities to prototype and research complex structures.

Figure 3. Relationship between toughness and stiffness for synthetic and biological materials. Note that engineering materials have a drastic decrease in toughness with an increase in stiffness while biological materials can maintain toughness despite an increase in stiffness until a critical value. Reproduced with permission.[15] Copyright 2015, Elsevier.

**ADVANCED
SCIENCE NEWS**
www.advancedsciencenews.com

**ADVANCED
MATERIALS**
www.advmat.de

Figure 4. Process map detailing steps in the use of additive manufacturing for exploring biological materials and bioinspired design.

In the field of biological materials science, AM is being used in two principal modes: a) to better understand the mechanical response of biological materials and to identify the governing mechanisms, and b) in the implementation of bioinspired designs. The use of AM to generate bioinspired materials and designs goes beyond the demonstration of principles. As **Figure 4** indicates that the 3D printing of prototypes is followed by mechanical testing, which provides guidelines for modifications and subsequent optimization. Since the synthetic materials used in AM have different properties than natural materials, the bioinspired design parameters must be modified accordingly. This sequential manufacturing and testing leads to a more complete understanding of the deformation, damage, and failure processes.

This overview is timely and focuses the attention of the materials community at large to this exciting new tool. Due to the vastness of the field of additive manufacturing and its recent advance, we do not include biomaterials and applications for biomedical engineering, such as tissue engineering, here. The reader is referred to reviews that extensively cover the recent advances of 3D printing in tissue engineering[17–23] and biomedical devices.[24–28]

2. Methods for Additive Manufacturing

A current challenge in materials science and engineering is the development of bioinspired materials containing unique heterogeneous architectures. In the past decade, additive manufacturing technology has been applied to fabricate bioinspired materials with complex geometries. Technology is being continuously updated to offer a versatile platform for fast and accurate fabrication on a small scale over large length-scale ranges.[29–33] The fundamental advantage of AM over traditional fabrication methodologies is the intrinsic ability to control the deposition both in space and local material composition. In this section, major AM methodologies used in fabricating bioinspired materials are presented and discussed. These include inkjet printing, direct ink writing, stereolithography, PolyJet (Stratasys Ltd.), two-photon polymerization, slip casting, and 4D printing.

2.1. Inkjet Printing

Inkjet printing provides a fast, flexible, and cost-effective technology for widely commercially available devices to construct

intricate structures.[34–36] Inkjet printing originated from 2D printing and was extended to three dimensions by the use of binding powders. During operation, solid powder particles are first placed on a platform. Liquid binding materials are then printed from the inkjet-printing head onto the powder to form one layer of the desired structure. After solidification, unbonded powders are removed and a second layer is deposited, followed by the layering of liquid binding materials by the print head. This procedure is repeated until the object is built. Support materials may also be used to fabricate samples with complex geometries.[37]

Compared to traditional manufacturing, inkjet printing offers precisely controlled local material composition through computer programming. This enables the fabrication of heterogeneous materials with well-controlled composition and properties.[31,37] An advantage of inkjet printing is the wide range of materials that it can deposit. Unlike photocurable inkjet printing, inkjet printing is not restricted to photopolymers. Additionally, inkjet printing is capable of printing multimaterials. Such a multimaterial fabrication process may generate a heterogeneous 3D material distribution of variable stiffness materials. This ability to print a distribution of variable stiffness materials is similar to strategies found in biological materials that contribute to enhanced strength and toughness. Inkjet printing is not limited to printing variable stiffness materials and can also print heterogeneous materials. One example of a popular inkjet-printing technique is fused deposition modeling (FDM). This technique heats thermoplastic filaments to their melting point and then extrudes, layer by layer, drawing cross sections of the desired object.

A drawback to inkjet printing is the additional processing steps that are needed to fully solidify the printed parts or improve surface finishes. In some cases, it is necessary to thermally cure or photopolymerize the inks after printing. Additionally, the surface roughness and quality typically need to be improved as a result of the layer-by-layer generation of the printed part.[38] Chemical or mechanical abrasions can be used to improve surface quality.

2.2. Direct Ink Writing

Direct ink writing, based on extrusion, is a successful technique to manufacture material systems with a wide range of geometries, sizes, and materials.[37,39,40] It is an extensively used AM technology due to its flexibility of both hardware and software combined with inexpensive materials and nozzles.[37] The direct-ink-writing system relies on a syringe nozzle to dispense material in the form of a continuous viscoelastic filament under controlled flow rates and along a digitally predetermined path. The rheological behavior of the ink, characterized by viscosity, mechanical yield stress under shear and compression, and viscoelastic response (i.e., the shear loss and elastic/storage moduli), can be tailored to suit specific applications.[39,41,42] For example, this can be applied to develop hydrogel scaffolds to guide cell growth.[39] The ink has to be sufficiently fluid to be printed out from the nozzle and, simultaneously, sufficiently stiff to form and hold the desired shape under gravity.[43] Therefore, the chemical and physical response of the ink, e.g., phase transitions and particle agglomeration, need to satisfy the rheological requirements.[41] The formulation of the ink should exhibit Newtonian flow when the gel is targeted, and
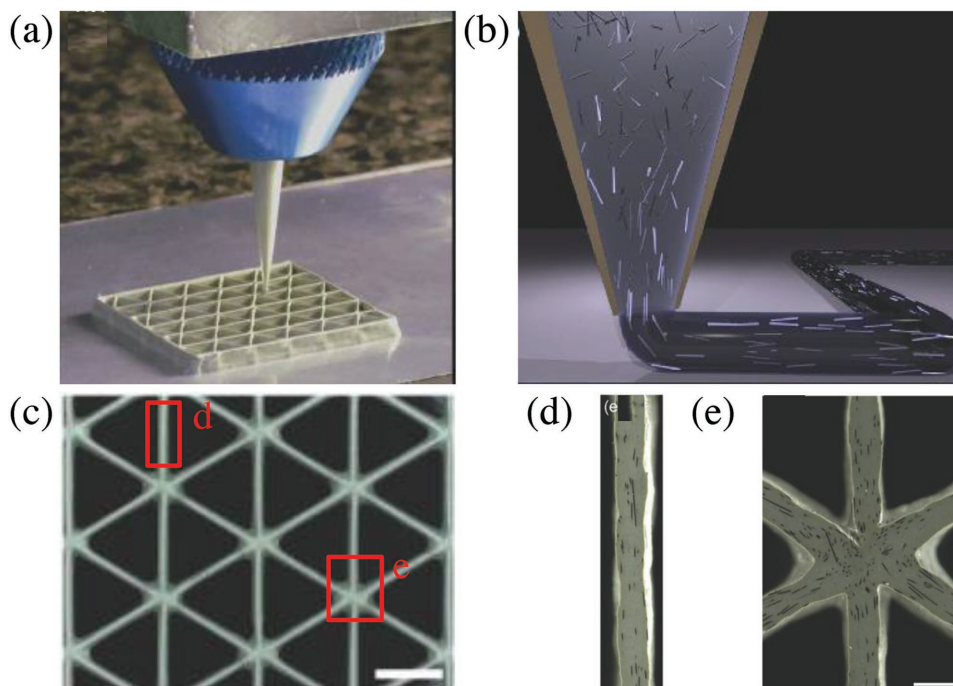
Figure 5. Fiber alignment in composite printing. a) 3D printing of a fiber reinforced composite. b) Illustration of the forced alignment of fibers due to shearing upon extrusion from the nozzle. c) Cellular 3D-printed prototype made of SiC-filled epoxy; scale bar is 2 mm. d,e) Alignment of carbon fibers along the print direction; the scale bars are 500 μm. Adapted with permission.[46] Copyright 2015, Wiley-VCH.

non-Newtonian behavior, sometimes with even a high Young's modulus, during the formation of spanning filaments.[44,45] Recent developments make the manipulation of anisotropic particles possible, and thus complicated bioinspired structures with multimaterials and anisotropy can be achieved.[46] **Figure 5**b shows the process of fiber alignment in composite deposition, whereas Figure 5d,e shows carbon fibers.

2.3. Photocurable Printing

Many AM techniques rely on photopolymers (thermosets) that, upon exposure to light, solidify and change properties. Most often, the light projected is ultraviolet (UV) light and can be sourced from a laser, lamp, projector, or light-emitting diode (LED). Polymerization of photopolymers relies on the addition of photoinitiators, which are molecules that produce reactive species when exposed to radiation. Photopolymerization is used in a layer-by-layer manner to generate 3D structures. This method is the most widely used in the generation of bioinspired structures discussed here. The following photopolymerization 3D processes are reviewed in this section: stereolithography, PolyJet multimaterial (Stratasys Ltd.), and two-photon polymerization, as they are among the most ubiquitous strategies in developing bioinspired prototypes.

2.3.1. Stereolithography (SLA)

Stereolithography is regarded as one of the first AM methods to emerge for the fabrication of light-induced polymerization, and

therefore has seen many advances.[47,48] Most of these advances are due to improvements in the laser performance with the thermosensitive polymer, which include depth of heating, pulse energy, and dwell time.[19] In SLA, an ultraviolet laser is employed to track the configuration of a 3D sample by focusing on the photoresin in a 2D plane. The polymerization is initiated upon illumination via a layer-by-layer mode (**Figure 6**).[49]

The addition of filler particles into the liquid resin makes it possible to additively manufacture polymer-based composites using stereolithography.[50,51] Although similar to direct ink writing, it is more restrictive in that it can only be used for photopolymers. This involves use of particles with ultrahigh response to magnetic fields within the reactive resin to provide control of the orientation of the particles.[52] Thus, based on this technology, bioinspired materials with complicated composite structures can be fabricated with reinforcements having controlled orientations. More specifically, this orientation control can be achieved by adding ultrahigh magnetic responsive particles into the reactive resin along with the implementation of an electromagnetic controller.[53] Another advantage of SLA is its ability to achieve high resolution. Resolution is dependent on the number of photons applied and some sophisticated setups such as Formlabs Form2 SLA 3D printers can achieve a resolution of 50 μm (**Figure 7**).[54]

A disadvantage of SLA is how slow it is relative to other AM methods due to its reliance on point-source illumination to pattern one volume unit at a time. Other AM techniques use other sources to project a mask pattern onto the liquid resin reservoir to solidify an entire layer at a time.[55] One of the greatest disadvantages of SLA for the development of bioinspired materials is the inability to print multiple materials in one sequence.
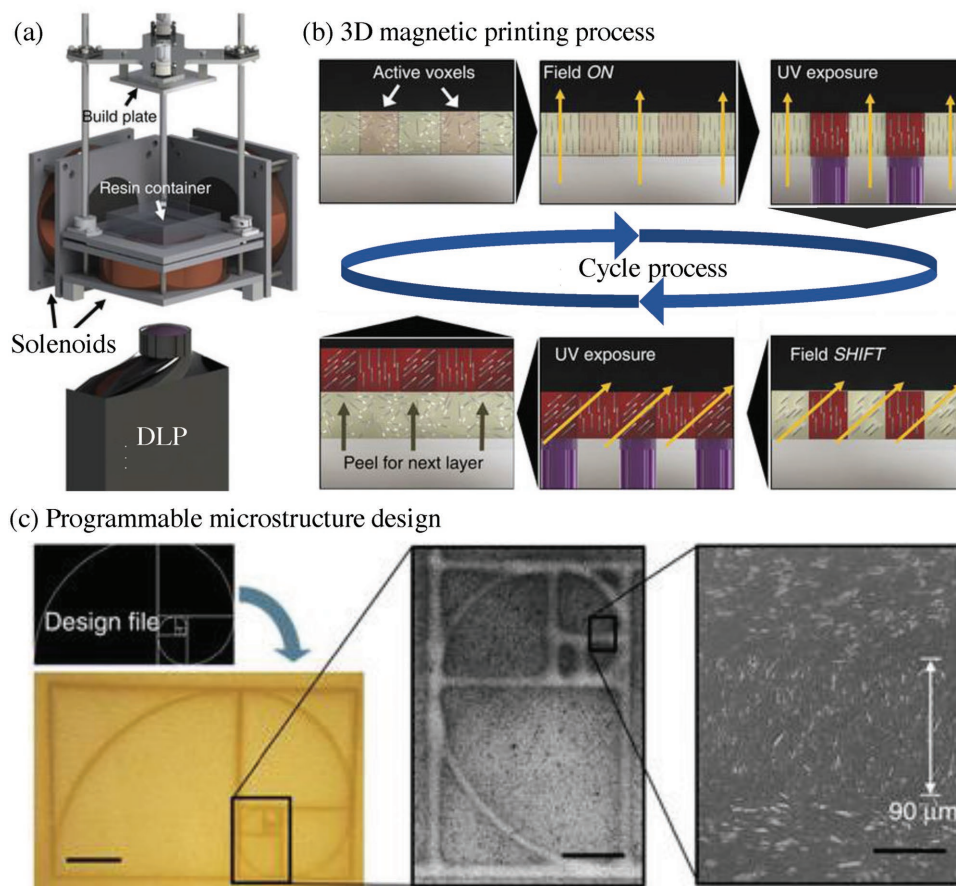
Figure 6. Details of the stereolithography technique adapted for magnetic printing. a) Stereolithography platform equipped with solenoids to magnetically control particle orientation and a digital light processor (DLP) to photopolymerize resin with ultraviolet. b) The 3D magnetic printing process achieves reinforcement by orientation of fibers within each layer of printed material based upon a shifting magnetic field. The build plate peels after a layer is complete to print additional layers. c) An example of reinforcement microarchitectures illustrating the golden rectangle. Clear feature sizes as low as 90 μm can be seen. Scale bars from left to right: 2 mm, 500 μm, and 50 μm. Adapted with permission.[49] Copyright 2015, Springer Nature.

2.3.2. PolyJet Multimaterial Technology (Stratasys Ltd.)

PolyJet multimaterial 3D printing was developed by Objet Geometries Ltd., which was later acquired by Stratasys Ltd. Unlike stereolithography, PolyJet selectively jets liquid photopolymer droplets that are immediately cured by ultraviolet lamps in a layer-by-layer fashion. This feature ensures that upon completion of the layer-by-layer process, the build is completely cured without the need to immerse the object in a bath of uncured material. This decreases the amount of time required. Most importantly, its ability to simultaneously jet-deposit multiple materials with different mechanical properties distinguishes it from traditional 3D-printing methods. There are eight printheads capable of printing up to three different materials, which can control local composition.[56] Both rigid and flexible materials can be printed simultaneously. This unique element is advantageous for the design of bioinspired materials that are often composites or have gradients
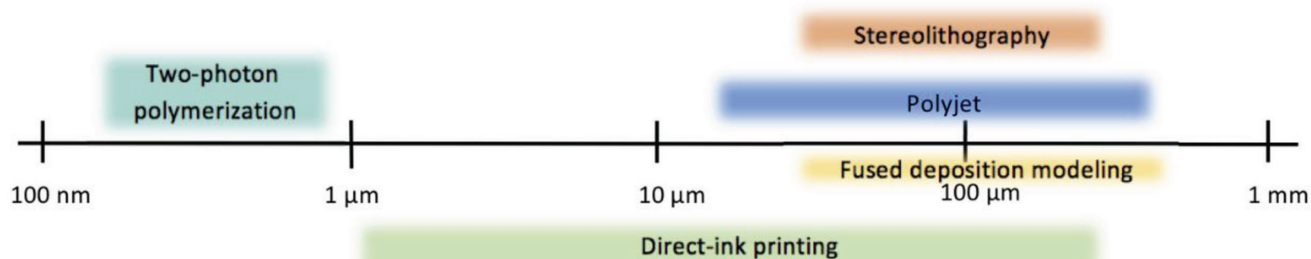
Figure 7. The minimum size ranges of features produced by principal AM printing methods. Adapted with permission.[55] Copyright 2016, Springer Nature.

1800940 (6 of 26)

**ADVANCED
SCIENCE NEWS**

www.advancedsciencenews.com

**ADVANCED
MATERIALS**

www.advmat.de

in material properties. PolyJet technology is able to achieve a high resolution of 600 dots per inch (dpi) and the thickness of each layer is 16–30 μm.[56] This resolution is compared to other AM techniques in Figure 7. Support material is needed to provide stability to jetted droplets and can be easily removed by hand or with a water jet. This technique is widely used to develop the bioinspired structures that are the focus here. A major reason for its popularity is its ability to print multiple materials simultaneously and its ability to produce high-resolution samples.

2.3.3. Two-Photon Polymerization

Two-photon polymerization is a microfabrication technique that uses ultrashort laser pulses to initiate two-photon absorption and subsequent polymerization of photopolymers.[57,58] Unlike stereolithography, resolutions beyond the diffraction limit can be reached due to the capabilities of strong laser pulse energy. Typical lasers that are used for this application are near-infrared Ti:sapphire femtosecond lasers.[57] This technology allows the ability to create design resolutions on the nanoscale, which distinguishes it from many other AM techniques. As shown in Figure 7, two-photon polymerization is able to achieve the smallest minimum size ranges of

patterned features.[55] It is important to note that when manufacturing at such a small scale, it is necessary to use highly accurate positioning systems, such as piezoelectric stages. This adds to the complexity of the 3D-printing system, which significantly increases its price. It is incredibly valuable to print on the nanoscale as it has been shown that enhanced properties of these biological structures are many times attributed to structures at the nanoscale.[32] Nanoscribe is one of the leading companies to utilize two-photon polymerization commercially and is a popular choice among the studies reviewed here that print nanoscale features.

2.4. Slip Casting

One of the bottlenecks to fabricating structural bioinspired materials is controlling the 3D orientations of highly anisotropic reinforcing particles. Orientation control leads to materials that are less vulnerable to impact damage with improved fatigue and load-bearing capabilities.[59] To tackle this problem, magnetically assisted slip casting was developed, combining traditional ceramic-manufacturing processes with layer-by-layer deposition of micro/nanoparticles and magnetic-field controls.[60] **Figure 8** shows the assembly method and the resulting structures. Reinforcing particles are
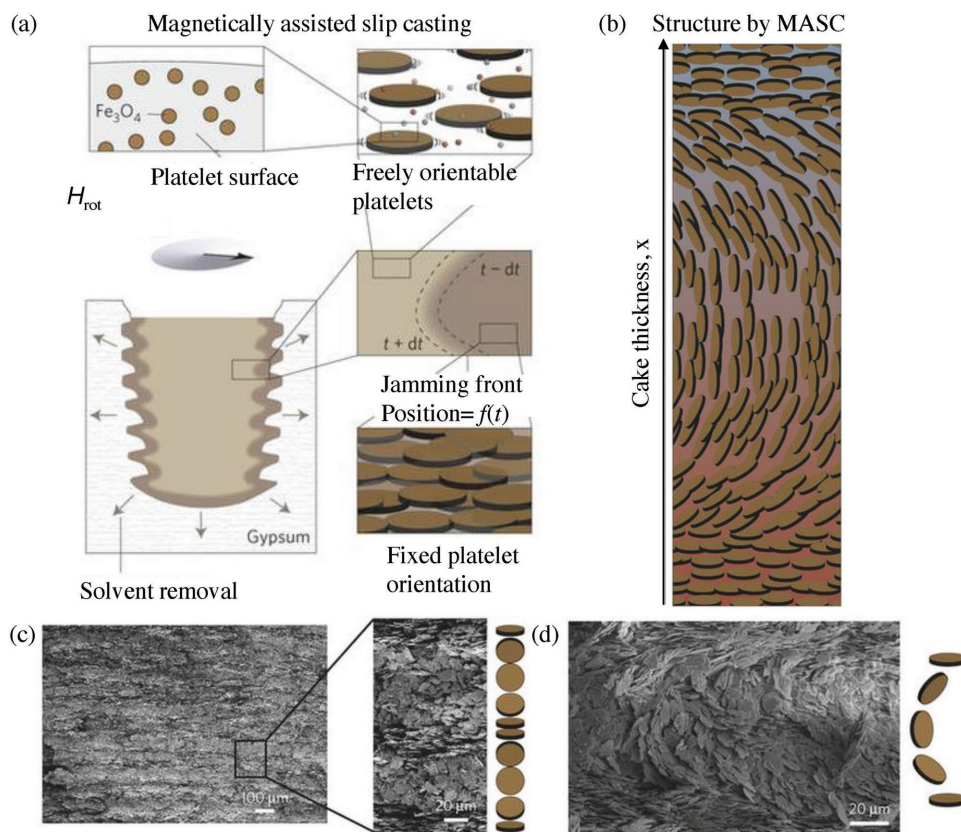
Figure 8. Assembly method and resulting structures of magnetic slip casting. a) Schematics illustrating the casting of magnetically aligned platelets from a suspension of alumina platelets coated with superparamagnetic iron oxide nanoparticles due to the rotation of an external magnetic field. The result is a complex-shaped porous mold. b) This illustration magnifies the ordering in response to a magnetic field (on the order of 500 μm). c,d) SEM images revealing the periodic platelet orientation pattern generated by magnetically assisted slip casting. Adapted with permission.[60] Copyright 2015, Springer Nature.

**ADVANCED
SCIENCE NEWS**

www.advancedsciencenews.com

**ADVANCED
MATERIALS**

www.advmat.de

coated with superparamagnetic nanoparticles to make them more responsive to the magnetic field. By employing this initial treatment, the reinforcing particles can be well oriented by a low-magnitude magnetic field.[61] To achieve a high concentration of oriented and aligned particle reinforcements, the fabricated structures are pressed and sintered to increase the density of particles within the matrix. This approach can be exploited to design and fabricate anisotropic composites with detailed microstructures.

2.5. 4D Printing

4D printing can fabricate structures with changeable geometries, configurations, properties, and functionalities.[62] These structures are space-dependent 3D-printed structures that are predictable in a controlled manner, providing a more representative prototype of many biological material systems.[63] Under an external stimulus, the proper combination of multiple smart materials acts cooperatively to motivate the printed structure to shift from one stable configuration to another.[64,65] The gradient structure brings distinctive advantages, e.g., significant volume reduction, self-assembly, multifunctionality, and self-repair, that are unique to many bioinspired designs. The basic idea of the working mechanism of 4D printing is illustrated in **Figure 9**.

A typical 4D-printing system may include a 3D-printing facility and a strong stimulus-responsive material. Additional mathematical modeling may be used to program the compositional changes and predict the shape-morphing abilities of the material. The stimulus must have the capability to trigger alterations of the printed structure, which may include light,[66] temperature,[67] water,[64] and magnetic fields.[65] Mathematical modeling plays a crucial role in 4D printing because it aims to establish the quantitative relations among material properties, material morphology, desired configuration, and stimulus properties. 4D printing provides a powerful platform for scientists and engineers to fabricate shape-morphing and gradient bioinspired materials. This is particularly important when mimicking the kinematics of stimulus-responsive plants, which is further explored in Section 3.7.
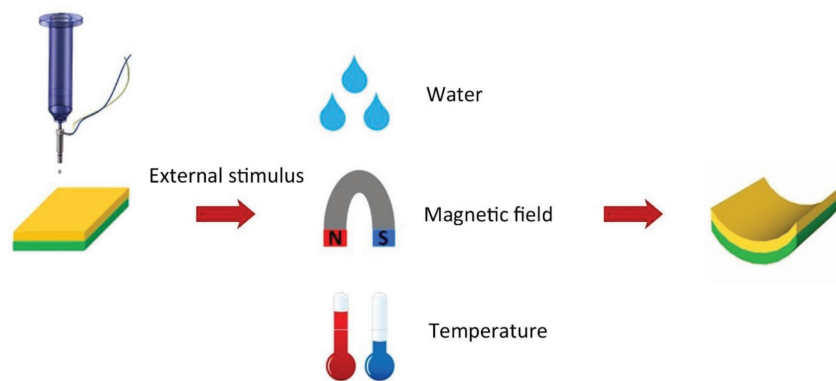
Figure 9. Schematic of 4D printing based on the deformation of materials by water, magnetic field, or temperature. Reproduced with permission.[64] Copyright 2016, Elsevier.

3. Additive Manufacturing of Design Motifs Found in Nature

Recently, there has been a surge in the use of AM in the field of biological materials science to both better understand the structure–property relationships of materials and their mechanical response, and to design bioinspired prototypes for optimized performance. The work reviewed here generally comprises five steps: 1) isolating a unique design motif found in nature, 2) templating the design with the use of micro-CT or self-generated CAD design, 3) generating the prototype via additive manufacturing, 4) mechanical testing the structure, and 5) optimization of its design. This sequence is illustrated in Figure 4, which was first discussed in Section 1. Additionally, theoretical and computational models are used to complement AM experimental results by providing supportive evidence and even going beyond the limitations of AM to extend the scope of the study. Additive manufacturing can provide a greater depth of knowledge when used in combination with theoretical and computational analyses. In this section, we review important accomplishments of AM in enhancing our understanding of biological materials through the facile generation of complex structures, which include composite/layered, hierarchical, suture, articulated, helical, cellular, and shape-morphing structures; and structured surfaces.

3.1. Composite/Layered Structures

The composite nature of biological materials is a leading feature that contributes to their exceptional resistance to damage. Therefore, it is desirable to both understand and replicate this structure synthetically. Bone and nacre are ubiquitous examples of biological composites and have inspired many studies. Multimaterial 3D printing enables the generation of variable stiffness composites necessary to fully characterize and explore the mechanisms at hand that promote damage tolerance.

Zhang et al.[68] investigated the damping effects of lamellar composites of staggered tablets consisting of a rigid plastic (VeroWhitePlus) and a viscous elastomer (D9680) inspired by the microstructure of bone[69] and nacre.[70] Prototypes were fabricated using the PolyJet multimaterial AM technique (Stratasys Ltd.), which was chosen due to its ability to simultaneously print a rigid plastic and a soft, viscous rubber. Three different brick-and-mortar designs were printed: 2D composite, 3D composite with square prisms, and 3D composite with hexagonal prisms, as shown in **Figure 10**a–c. This study determined how the geometry and volume fraction of composites affect damping properties, such as the loss modulus (E''), to better predict the material's ability to dissipate energy.

Dynamic testing of the 3D printed prototypes revealed an increase in the loss moduli when compared to their constituents (Figure 10d). This suggests that the composites have an enhanced mechanism to dissipate energy. This is due to a large shear

**ADVANCED
SCIENCE NEWS**
www.advancedsciencenews.com

**ADVANCED
MATERIALS**
www.advmat.de
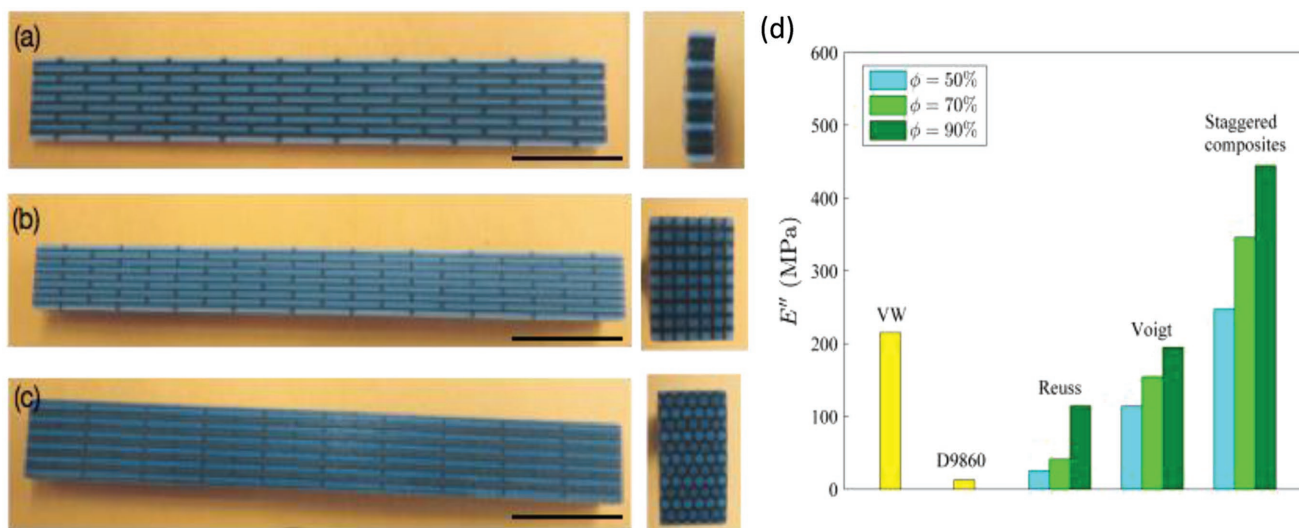
Figure 10. Staggered polymer composites manufactured by PolyJet 3D printing with two polymers VW (light color) and D9860 (dark color). a) A 2D composite with a brick-and-mortar structure (scale bar: 20 mm). b) A 3D composite with square prisms (scale bar: 20 mm). c) A 3D composite with hexagonal prisms (scale bar: 20 mm). d) Comparison of constituents (VW and D9680) with Reuss, Voigt, and staggered composites with various volume fractions corresponding to the volume fraction of the rigid plastic. Adapted with permission.[68] Copyright 2015, Elsevier.

deformation of the viscous material in conjunction with the high stiffness of the hard phase. There is a competition between the deformation of the hard (discontinuous) phase and the soft (continuous) matrix. The 3D structures outperformed the 2D structure due to higher loading transferability. The 2D model suffers from low loading-transfer ability because the loading transfer occurs by shear only between the platelets. The 3D staggered composites have a more complex topology (square and hexagonal shaped prisms) that can transfer the load. For example, the square prism arrangement is able to induce shear stress on all four of its lateral surfaces. Changing the shape from square to hexagonal did not have a considerable effect on the loss modulus, which suggests that this property is more strongly determined by volume fraction. It was shown that by increasing the volume fraction of the rigid polymer, from an initial value of 50% up to a critical value (≈90%), the loss modulus increased, enhancing the damping properties (Figure 10d). Beyond 90%, the damping is dominated by the high stiffness component. In this case, AM helped quantify the geometric and volume fraction constraints for enhanced damping of lamellar composites having staggered tablets.

Dimas et al.[71] investigated the fracture response in three different bioinspired layered composite materials: bone-like, biocalcite-like, and rotated-bone (helicoidal with sequential layers at different angles to the longitudinal axes), mimicking the osteon[1] structure. Comparing the three different architectures provides insight into the role that geometry plays in organizing stiff and soft phases. All composites were made using the PolyJet multimaterial 3D-printing technique (Stratasys Ltd.) with 70% volume fraction of the rigid plastic and 20% volume faction of the softer phase. Deformation and fracture mechanics testing were performed on the three prototypes and compared to bulk samples of each constituent. As expected, the composites outperformed their constituents, which is attributed to geometrical toughening. Toughening occurs due to the introduction of a significant stiffness mismatch, which allows the crack to propagate through the more compliant material.

The path that the crack travels is dictated by the topology. Each AM material was compared to a complementary computational study to visualize and expand upon the toughening mechanisms discovered experimentally.

The bone-like topology, which can be described as a brick-and-mortar-like structure with stiff plates in a compliant matrix, generates significant delocalization of stress and strain (**Figure 11**a,b). The compliant phase is continuous throughout the sample, which allows it to distribute stress and strain more effectively. During the initial stages of crack propagation, nonlocalized failure occurs in the vertical compliant phase, while the horizontal portion undergoes shear strain holding the system together. The AM samples did not fail at the interfaces, which suggests that interfacial adhesion is sufficiently strong to keep the constituent materials together. The initial stages of crack propagation are nearly identical to the simulation (Figure 11a,b). These similarities support that the bone-like topology induces significant stress and strain delocalization. However, the experiment and the simulation differ upon further crack propagation. This is attributed to crack propagation inducing nonlinearities, in the AM experiment, which cause nonuniform loading and different stress fields to occur in the crack tip region. The computation, however, maintains constant boundary conditions, so that these nonlinearities are not observed. Deviations between the experiment and computation highlight that nonlinearities dominate as the crack propagates.

Rotated bone-like topology has an initial characteristic zigzag fracture path through the compliant phase, which is able to continuously transfer longitudinal strain (Figure 11c). This is seen in both the experimental and computational systems. It is more energetically favorable for the crack to propagate in the compliant matrix, which forces it to take a longer path and induces toughening. The material is able to sustain increased deformation after significant loading due to delocalization of the soft matrix upon the onset of crack-tip blunting. Similar to the bone-like model, the rotated-bone like experiment deviates

**ADVANCED
SCIENCE NEWS**
www.advancedsciencenews.com

**ADVANCED
MATERIALS**
www.advmat.de
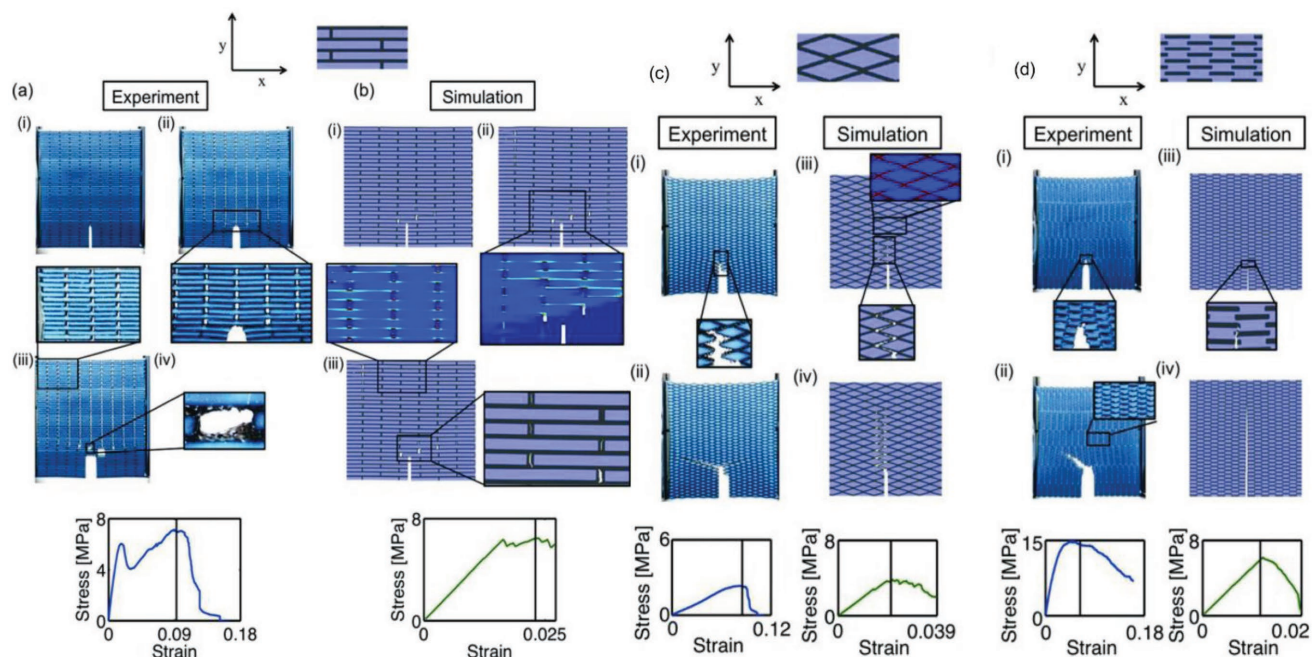
Figure 11. Comparison of deformation and fracture mechanisms in AM samples and simulation. a) The 3D-printed bone-like structure. b) Simulation of the bone-like topology. c) The rotated-bone-like structure. D) The biocalcite-like structure. i–iii) Evolution of fracture in both samples over time. Adapted with permission.[71] Copyright 2013, Wiley-VCH.

from the simulation as crack growth proceeds. Again, this is attributed to a change in boundary conditions due to nonlinearities in the experiment that do not exist in the simulation.

In the biocalcite-like topology, unlike the bone-like and rotated-bone-like, the stiff component is the continuous matrix, not the soft phase. This did not enable the crack to propagate continuously through the soft phase resulting in a different fracture mechanism. The crack no longer meanders through the compliant matrix, but results in a rugged fractured surface as it attempts to minimize the distance it travels. This is verified visually by the simulation (Figure 11d). It is important to note that the biocalcite-like topology accrued significant flaws due to inaccuracies in printing. This accounts for the differences in failure observed in the experiment and the simulation (Figure 11d).

The composite shells of abalone[3,70] and nautilus[72] have a distinctive architectural feature, the mineral bridges,[4] which are known to enhance stiffness, strength, and toughness.[69,73] Gu et al.[73] investigated the effects of varying the volume fraction of the stiff and soft component and the number of mineral bridges to understand the role that geometry plays in fracture toughness. PolyJet technology multimaterial AM was used to fabricate composites with a brick-and-mortar pattern consisting of two vastly different constituent materials: stiff and soft. Five different volume fractions of the stiff component were studied (50%, 60%, 70%, 80%, and 90%) with variation in the number of mineral bridges per unit (6, 9, 12, 15, and 18). Tension tests on single edge-notched samples were performed with digital image correlation (DIC) to determine strength and toughness and visualize strain fields. The prototypes enabled a better understanding of the failure mechanisms (**Figure 12**). The addition of mineral bridges was determined to play a crucial role in crack deflection, which increased the strength and toughness.

The portion of this study that focused on the effects of volume fraction highlights a combination of toughening mechanisms leading to successive crack deflections that work synergistically to increase the fracture toughness. At 90% volume fraction of stiff material, the sample fails in a brittle fashion with low failure strain and high failure stress, similar to the bulk material. This is due to the limited soft matrix available to allow for crack propagation. The volume fraction of 70% has the highest failure strain and 80% has the highest failure stress. Typically, the samples with the highest toughness and strength rely on a generous volume of stiff material (70–80%) with enough compliant material to deflect the crack leading to nonbrittle behavior. When traveling through the compliant material, the crack gets deflected by discontinuous geometries. This results in a zigzag pattern. This is similar to the results by Zhang et al.[68] that suggest with increasing volume fraction of the stiff material, toughness increases until a critical value is reached.

The addition of mineral bridges (stiff material that disrupts the continuity of the soft matrix) affects crack propagation for each volume fraction differently. Addition of mineral bridges to the 80% sample resulted in a response more similar to the bulk stiff material with very small deflections along the bridges in a saw-tooth path. The 50% sample benefited from the addition of mineral bridges as they enabled more crack deflection pathways resulting in a blockwise path. The blockwise path is a desirable failure pattern as it is associated with an increase in strength for the composite topologies studied and is even seen in natural nacre. Increasing the number of mineral bridges increases the toughness until a critical limit is reached (roughly nine per tile as determined by this study) when brittle failure starts to occur. If there are too many mineral bridges the domain of the soft

**ADVANCED
SCIENCE NEWS**

www.advancedsciencenews.com

**ADVANCED
MATERIALS**

www.advmat.de
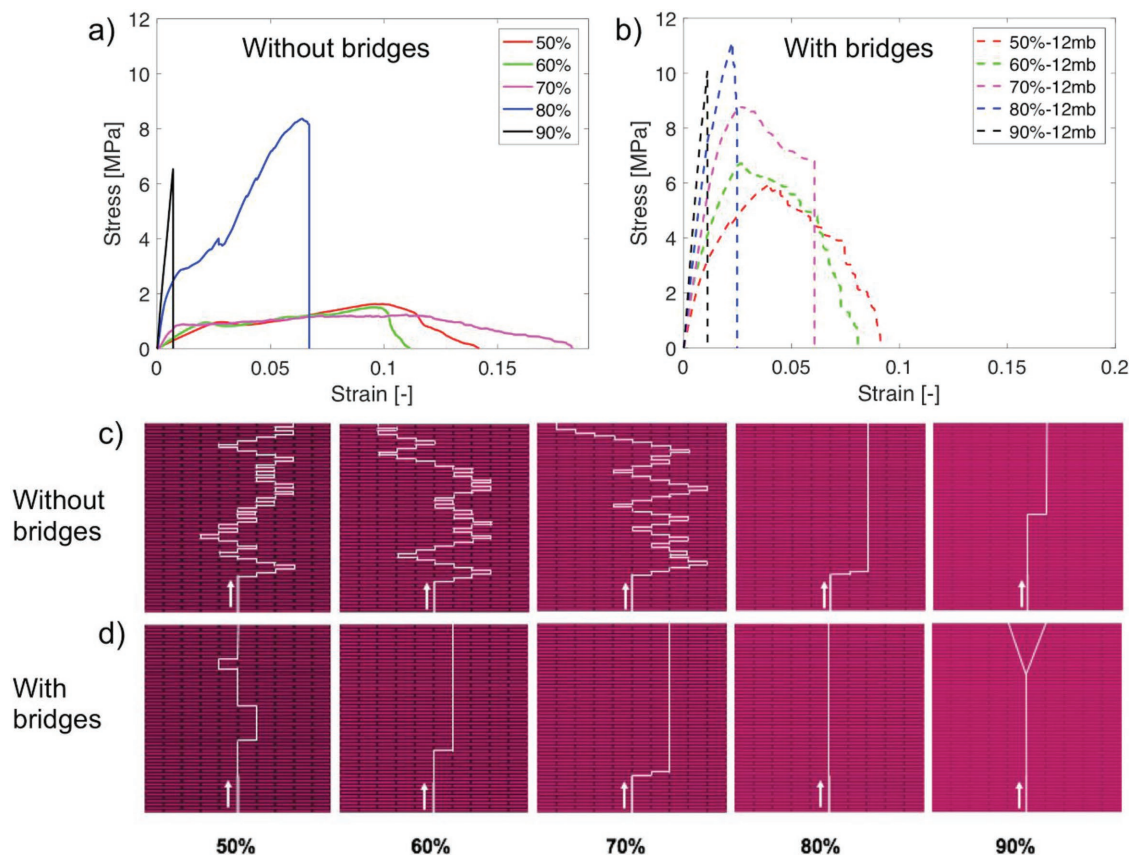
Figure 12. Comparison of material response with variations in mineral bridge content and volume fractions of stiff material. a) Stress–strain plots for various volume fractions of stiff material without mineral bridges. b) Stress–strain plots for various volume fractions of stiff material with 12 mineral bridges. c) Crack propagation without mineral bridges for various volume fractions of stiff material. d) Crack propagation with mineral bridges for various volume fractions of stiff material. Reproduced with permission.[73] Copyright 2017, Elsevier.

matrix will be restricted limiting the shear length. While it has been known that mineral bridges contribute to the strength of nacre, AM enabled the performance of a systematic study. This systematic study was accomplished with PolyJet technology's multimaterial printer and the ability to strongly control design parameters such as geometry and architectural features of the mineral bridges.

Yet another distinguishing aspect of nacre is the shape of the tablets, which was first described by Barthlelat and Rabiei[74] as having an irregular thickness that is accommodated by the adjoining layers. This is thought to contribute to nacre's high strength and toughness despite having relatively weak constituents.[72] Espinosa et al.[75] used AM to determine that the dominant toughening mechanism is due to the brick morphology (waviness) and its ability to dissipate energy during sliding. This previously hypothesized toughening mechanism benefited from AM as a key method to provide credence. The brick-and-mortar-like microstructure was replicated and scaled up using fused deposition modeling. An important consequence of scaling up was the elimination of smaller-scale surface roughness. This allowed the waviness of the nacre to be studied in isolation. Rather than mimicking the random waviness seen in natural nacre, Espinosa et al.[75] used a dovetailed tablet structure to parametrically study the angle and length of the dovetail (**Figure 13**). The dovetailed tablet structure is

composed of acrylonitrile butadiene styrene (ABS), a rigid polymer that mimics the inorganic material (aragonite) found in nacre, and the interfacial gaps between the tablets are filled with Dow Chemical flexiblized epoxy, which is analogous to the organic matrix (chitin).

Prototypes were fabricated with varying dovetail angles (θ) and overlap lengths (L), and prenotched samples were tested in three-point bending and postprocessed with DIC to quantify tablet sliding. This information ultimately enabled an understanding of how the angle and length influences performance and deformation mechanisms. The angle ranged from 0° to 3°, while the overlap length was either 2.1 or 5.7 mm with a constant thickness of 1.855 mm for all samples. Tablets with no dovetails ($\theta = 0°$) demonstrated negligible hardening after yielding due to the lack of an interfacial hardening mechanism. Tablets with a dovetail with $\theta = 1°$ showed an improvement in highest stress and strain before failure (greatest degree of sliding) and greatest energy dissipation per unit volume of more than 100% when compared to the $\theta = 0°$ tablet. This is attributed to the interfacial hardening effect, which describes significant hardening following the onset of sliding. As the tablets slide past one another, they must overcome the waviness, which causes them to interlock and increase resistance to sliding. Shorter dovetail lengths had dramatically less energy dissipation. This caused softening and tablet pullout to occur
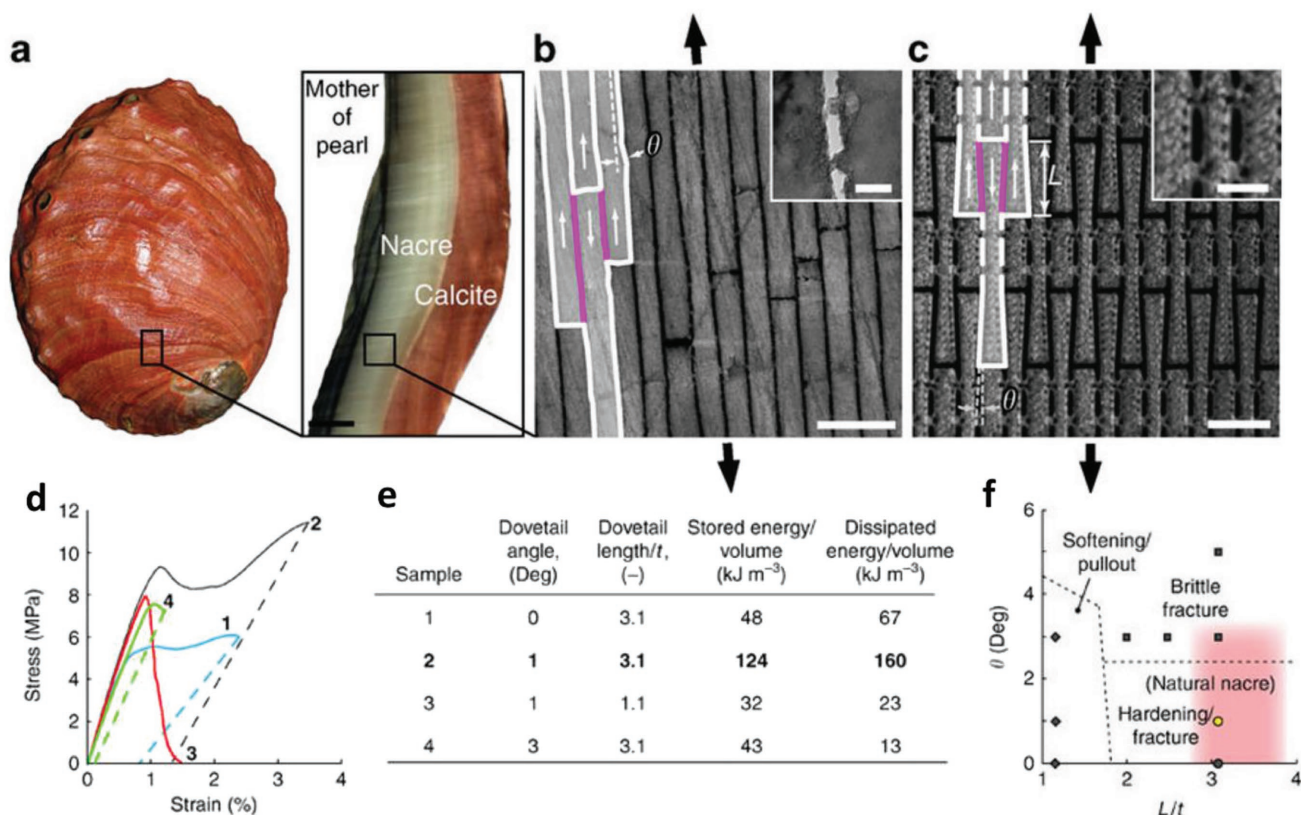
Figure 13. From natural nacre to bioinspired prototype to determine failure modes. a) The shell of a red abalone with a cross-section cut from the shell showing the nacre (white). b) SEM image of the natural nacre highlighting the waviness of the brick-and-mortar-like micro/nanostructure (scale bar: 1 μm). For clarity, a set of tablets is outlined in white. The overlap region is highlighted in magenta. This is where relative sliding occurs. The inset shows a TEM image of the mineral bridges (scale bar: 100 nm). c) Bioinspired nacre composite with dovetailed tablets before polymer infiltration. The length, L, and angle, θ, of the dovetail in the overlap region are studied parametrically (scale bar: 5 mm). The inset shows the detail of the mineral bridges (scale bar: 2 mm). d) Engineering stress–strain curves for bioinspired prototype of the four samples shown in (e). e) Table describing the four samples with various dovetail angles and lengths and their corresponding stored and dissipated energies. f) Map of failure modes for each of the four samples. Sample 2 is shown in yellow and has the highest stored and dissipated energy and fails by the same mechanism found in natural nacre (highlighted by the red area). Reproduced with permission.[75] Copyright 2011, Springer Nature.

at lower stresses and strains. These failure modes are mapped out in Figure 13f. Similar to the natural nacre in their study, the printed samples had sliding only in the overlap region between tablets. The sample that exhibited similar failure modes as natural nacre had the highest stored and dissipated energy per volume (Figure 13e). Agreement between the biological nacre and the bioinspired prototype provides evidence that the primary mechanism for an increase in strength and ductility is due to the interfacial hardening.

The work using AM bioinspired prototypes on the morphology of the brick-and-mortar-like microstructure of nacre inspired a computational study to further verify that the interfacial hardening mechanism was the dominate driving force for increased strength and toughness. Rim et al.[76] used dimensional analysis and parametric studies to determine an optimal morphology that was shown to increase energy dissipation over 70 times. This computational study was able to go beyond the extent of the AM study, as it was not limited by the properties of the material used or the number of critical features studied. Several critical features of nacre were investigated that included geometric (dovetail angle, tablet length, length of overlap between tablets, tablet thickness, and bridge thickness)

and material properties (modulus of tablet, modulus of filler, and filler yield stress). In general, the work accomplished by Rim et al.[76] demonstrates that different composite behaviors and dissipation energies can be obtained with even the slightest change in a single geometric or material property. In this study, computational analysis was not only used to verify what was learned in the AM experiment but also to expand upon the initial discovery. Multiple relationships between geometric and material properties were presented to show their effects on the toughening mechanisms. This highlights how AM can be used in combination with simulations and experiments to develop a more sophisticated understanding.

3.2. Hierarchical Architectures

Meza et al.[77] explored the mechanical robustness and damage tolerance of hierarchically designed nanolattices inspired by nature with the use of two-photon polymerization (Nanoscribe). While this study does not draw inspiration from a specific biological material, it has been included here as it highlights a fundamental motif found across a diverse range of exceptionally

resilient biological structural materials, such as bone, sponges, and wood.[78,79] It is important to better understand how hierarchical levels function as a network at the nanoscale to improve and tailor design concepts for damage tolerant engineered structures. In this study, hierarchical nanolattices were designed with various orders of hierarchy which led to the discovery of a unique range of tailorable properties for resilient hierarchical-structured metamaterials.[77] All fabricated samples were designed using the octahedron as the repeating unit at three hierarchical levels: the first order is an octahedron with an elliptical beam repeat unit; the second order is an octahedron of octahedra with the first-order octahedron as a repeat unit; and the third-order is an octahedron of octahedra of octahedra where the second order as the repeat unit. Along with different orders of hierarchy, three different combinations of materials were studied. This includes solid polymer, hollow ceramic (Al_2O_3) with 20 nm wall thickness, and core–shell polymer/ceramic composite (**Figure 14**).

In situ nanomechanical compression experiments performed on second-order and third-order structures were used to determine the effect of hierarchy on strength and stiffness, recoverability, and failure. Linear scaling of stiffness and strength with density was observed in the hollow ceramic from transition of the first hierarchical level to the second. Simulations were additionally performed to confirm that linear scaling

is attributed to axial load distribution among the beams. Excellent recoverability of the hollow ceramic (Al_2O_3) was observed as shown in Figure 14. Again, the structure efficiently distributes the load within each hierarchical level. Nonaxially orientated beams either bend or undergo elastic buckling to accommodate large global deformation without failure. Failure occurred through a combination of mechanisms including: elastic beam buckling, shell wall bending, brittle fracture, and viscoplastic yielding. This study highlights how AM can produce bioinspired hierarchical nanolattices that are ultralightweight, recoverable, and have a near-linear scaling of stiffness and strength with density. AM has provided the opportunity to engineer materials on a fundamental nano-length-scale which not only enhances our understanding of structure–property relationships but enables the generation of highly tailorable materials.

Gu et al.,[80] inspired by the hierarchical structure of the conch shell,[81] developed 3D biomimetic prototypes and performed mechanical testing to elucidate the crack arresting mechanisms that enable its damage-tolerant capabilities. The conch shell has a cross-lamellar structure with alternating sheets of mineralized calcium carbonate separated by an organic layer of protein. The cross-lamellar structure has three levels of hierarchy that work synergistically to delocalize damage. This provides a template for multimaterial AM of the
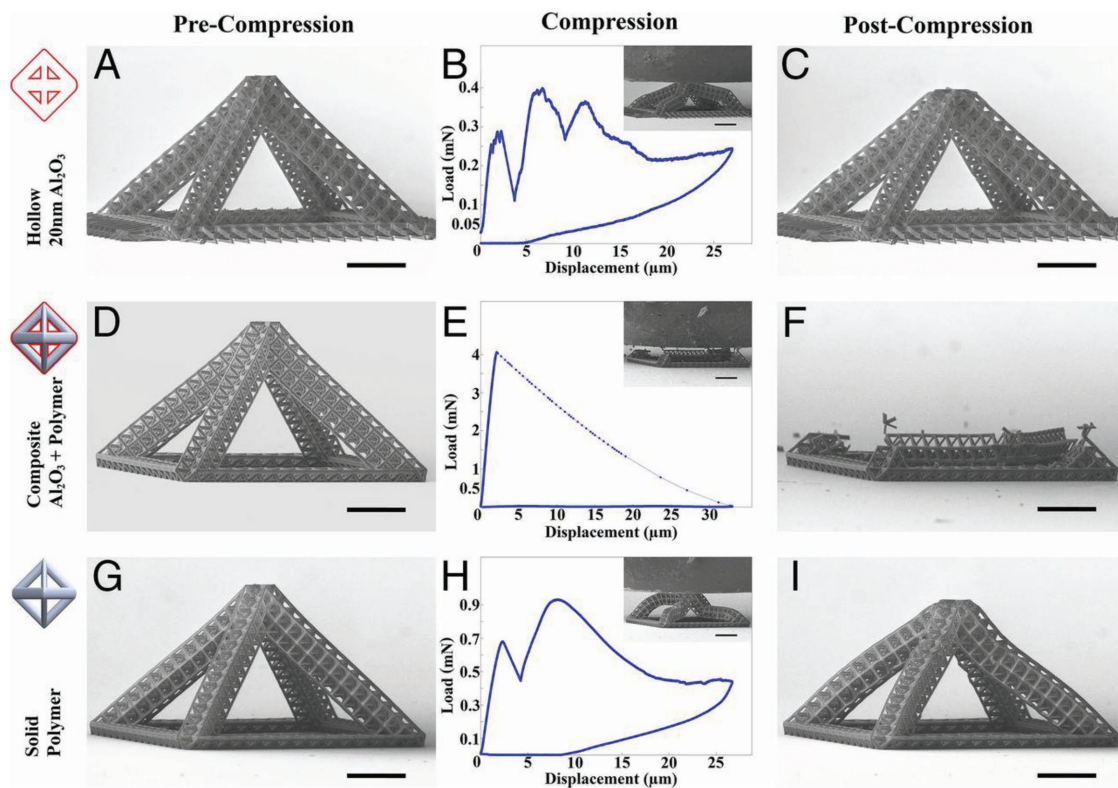
Figure 14. Compression experiments and response on second-order hierarchical architectures. a) Image of the hollow ceramic sample before compression. b) Load displacement of compression to 50% strain. c) Postcompression of the hollow ceramic showing recoverability. d) Image of the polymer and ceramic composite before compression. e) Load displacement of compression to 65% strain. f) Postcompression of the composite sample showing catastrophic failure. g) Image of the polymer sample before compression. h) Load displacement data of compression to 50% strain. i) Postcompression of the polymer sample (scale bars: 20 μm). Reproduced with permission.[77] Copyright 2015, National Academy of Sciences, USA.

**ADVANCED
SCIENCE NEWS**

www.advancedsciencenews.com

**ADVANCED
MATERIALS**

www.advmat.de
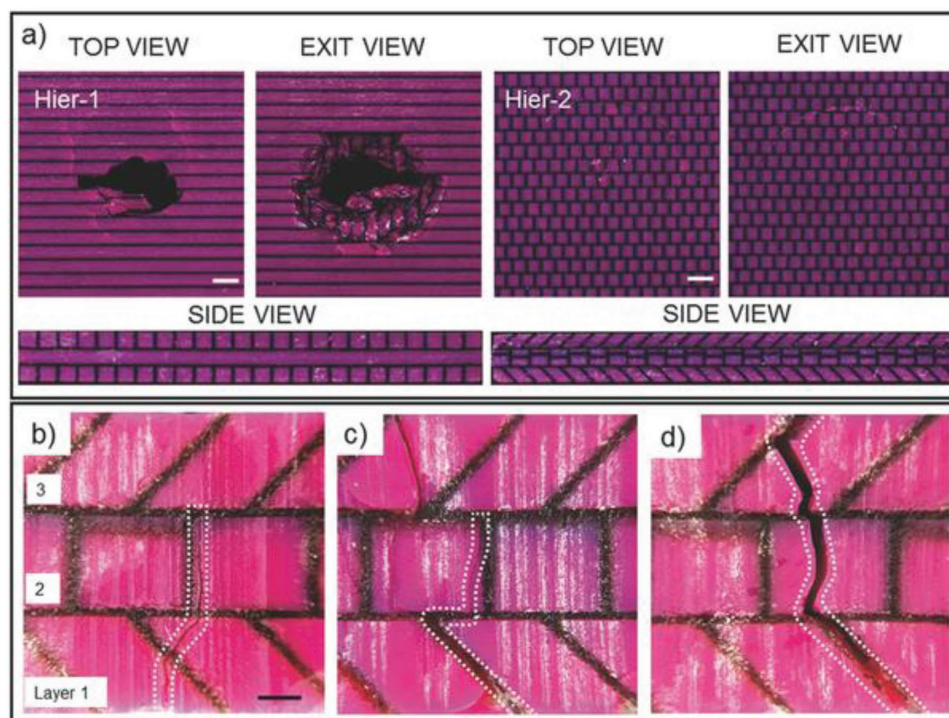
Figure 15. Comparison of damage mechanisms between Hier-1 and Hier-2 structures with an impact velocity of 3 m s^{-1}. The stiff material is denoted by pink, and the soft material is denoted by black. a) The Hier-1 composite fails catastrophically, while Hier-2 responds by generating cracks. Scale bar: 3 mm. b) Image of a cross-section of Hier-2 showing crack propagation and arrest by the second layer. Scale bar: 1 mm. c) Image of a cross-section of the same sample with a different crack that meanders along the soft interface and changes direction when reaching the interface between the first and second layers. d) Another cross-sectional image of the same sample where an additional crack propagates and terminates in the third layer due to sharp angle at the "criss-cross." Reproduced with permission.[80] Copyright 2017, Wiley-VCH.

layered composite, which was accomplished using a Stratasys Connex 3 multimaterial printer with PolyJet technology. Two levels of hierarchy were built to investigate the effect of increasing the order of hierarchy (**Figure 15**). The Hier-1 design only includes a single order of hierarchy, which does not have the cross-lamellar feature, while Hier-2 has an increased level of hierarchy, which includes the cross-lamellar structure. This work is made possible by the ability of AM to capture the complexity of the hierarchical structure.

Each prototype was tested for impact performance using a drop tower with various incident velocities. This provides insight into how hierarchy affects critical impact energy and stiffness. As predicted, the Hier-2 prototype outperformed Hier-1 due to an increase in interfaces that enables crack mitigation by forcing an incoming crack to change direction. Analysis of each prototype after drop-tower testing illuminates the damage mechanisms that explain the increase in performance with increasing hierarchy. The Hier-1 is only able to stop the impact of the projectile at a velocity of 2.3 m s^{-1}, while the Hier-2 prevents the projectile from penetrating for each velocity. Hier-2 in most cases is able to stop the crack from reaching the third layer by restricting the path of the crack to the soft phase, as shown in Figure 15. The complexity of the organization of the stiff and soft material in a criss-cross lamellar structure, which increases the interfaces, forces the crack to constantly change direction leading to energy dissipation.

3.3. Suture Interfaces

Sutures are a fundamental design motif found in nature consisting of compliant interlocking seams that connect stiffer components. They are found across a diverse range of biological materials (boxfish plates,[82] skull bones,[83] and turtle shells[84,85]) and contribute to the remarkable mechanical properties such as stiffness, strength, and toughness of such materials. Sutures can enhance the functionality of inherently brittle materials. It has been known that the geometry of the suture interface influences the mechanical properties. 3D printing has been recently utilized to identify the geometrical effects of sutures and validate analytical and computational models.[86,87]

An important feature of sutures is the nonlinear traction behavior that occurs due to frictional pullout of the interlocking structures, which accounts for strength and energy absorption. Malik et al.[86] characterized the pullout response of an interlocking jigsaw-like suture using AM and mechanical testing to verify and optimize analytical and finite element models. Jigsaw-like interlocked sutures were fabricated using digital light processing technology (Micro HiRes Machine, Envision-Tech) made with ABS (a relatively brittle polymer) with different interlocking angles: $\theta = 5°$, $10°$, $15°$, and $20°$ as shown in **Figure 16**. This particular AM technique was used as it has very high resolution to produce smooth surfaces, which was important when exploring the suture interfaces.
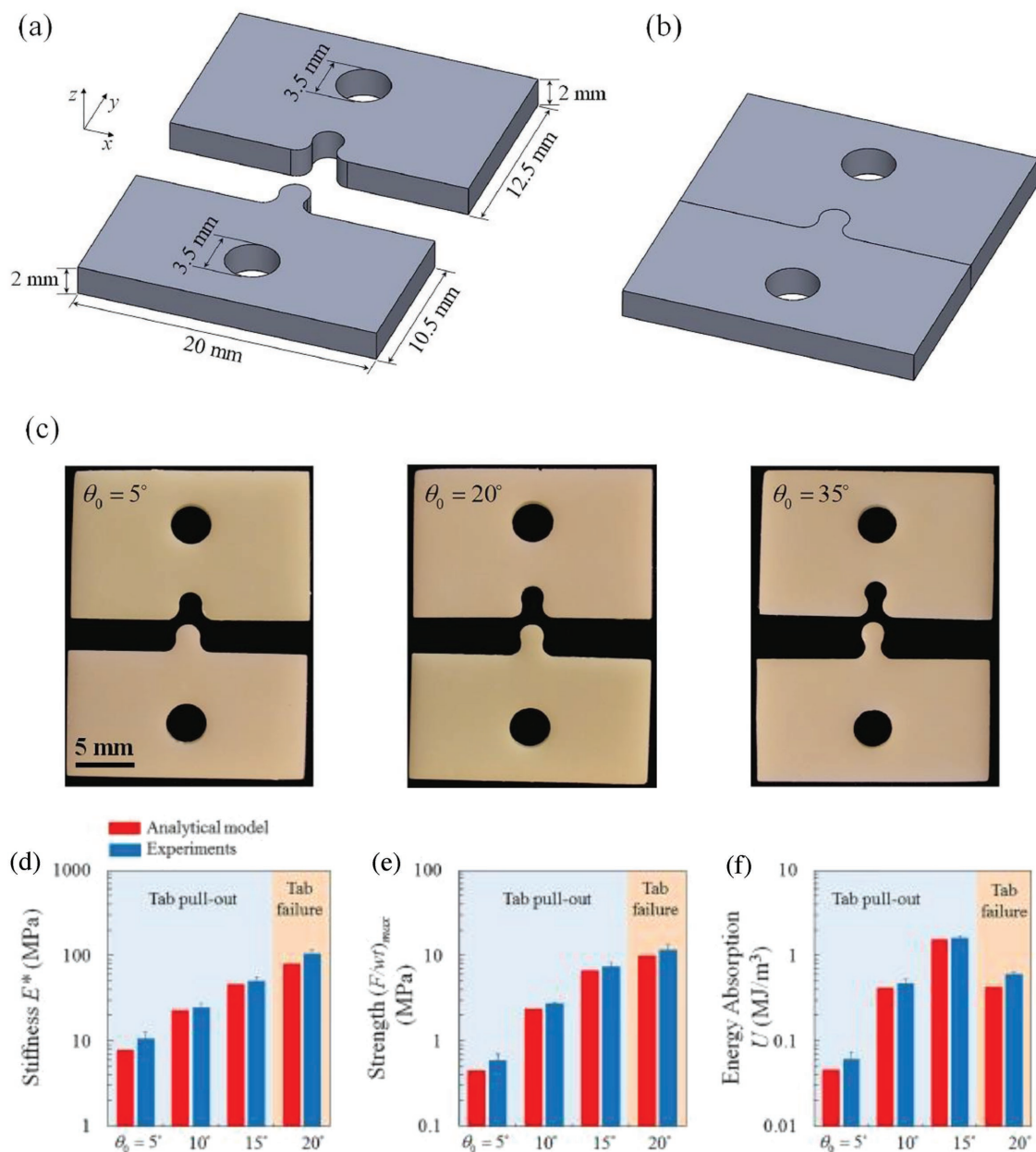
Figure 16. Examples of "jigsaw" sutured samples. a) CAD design of the "jigsaw" pieces of the sutures. b) Interlocking mechanism of the sutures. c) Images of 3D-printed prototypes with interlocking angles of 5°, 20°, and 35°. d) Stiffness as a function of interlocking angle. e) Strength as a function of interlocking angle. f) Energy absorption as a function of interlocking angle. Reproduced with permission.[86] Copyright 2017, Elsevier.

Mechanical pull tests were performed and forces and displacements were measured to determine the full pullout response in terms of stiffness, strength, maximum elongation, and energy absorption and the effect of the interlocking angle.[86] It was shown that, as the interlocking angle increased the stiffness, the strength, maximum elongation, and energy absorption all increased up to a critical angel (Figure 16). The highest angle (20°) fractured prematurely and showed cracks initiating at the edges of the contact region. The increase in strength with an increase in interlocking angle can be attributed to geometrical interlocking, which resists pullout as the tabs stay in contact over a longer pullout distance.

Finite element simulations were used to validate the mechanisms explored in the AM samples and to develop a platform that can be used to study more complex structures by including analysis of the coefficient of friction. This is a common trend, which involves using simulations to go beyond what is learned from the AM models. Their procedure tested 80 combinations of interlocking angle and coefficient of frictions. Increasing either the interlocking angle or the coefficient of friction improves the pullout response, but, as a consequence, introduces undesirable tensile stresses. Therefore, there exists an optimal angle and coefficient of friction that can maximize the pullout response. The optimization results

for stiffness, strength, and extension showed that a maximum occurs when the coefficient of friction is zero and the interlocking angle is 13°. This occurs because the elimination of friction reduces tensile stresses. However, this optimization is not beneficial for energy absorption, as friction is a predominant mechanism to absorb energy, which results in poor toughness.

Overall, this study used AM to generate tailored geometries to better understand the pullout response in relation to stiffness, strength, elongation, and energy absorption. AM provides a robust platform to validate and optimize models of complex geometries to provide greater insight into the fundamental mechanisms that account for the remarkable properties of suture-like features biological materials.

The capabilities of AM to generate detailed geometries has advanced our understanding of the role geometry plays in suture interfaces which allows for tunable deformation. Sutures, inspired by diatoms,[88] with generalized trapezoidal interlocking features (**Figure 17**) were manufactured using a PolyJet multimaterial printer with design parameters of bonded versus unbonded, tooth tip angle, and shape factor (trapezoidal, antitrapezoidal, and rectangular).[87] Through augmentation of each design parameter, a wide range of stiffness, strength, and toughness can be achieved. It was shown that the tip angle and geometry control the stress distributions within the interfacial layers, which command the failure mechanisms. In response to shape factor, rectangular interfaces fail due to shearing. Trapezoidal and triangular interfaces fail due
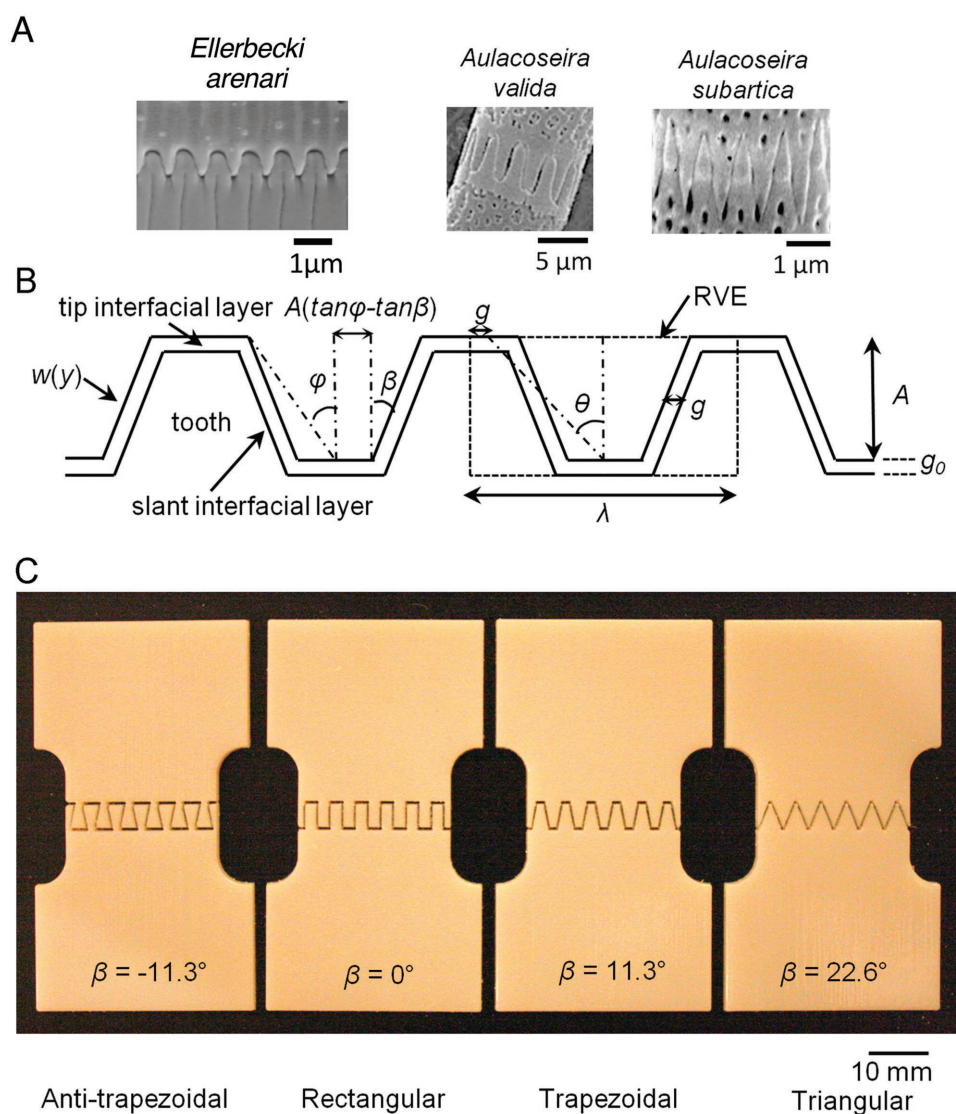
Figure 17. Comparison of inspiration from nature (diatoms), design, and the resulting 3D-printed prototypes. a) Images of suture interfaces of diatoms. b) Design of general trapezoidal suture interfaces with defining geometric parameters. c) Images of various geometrically bioinspired 3D-printed suture prototypes. Reproduced with permission.[87] Copyright 2014, Elsevier, wherein the *Ellerbecki arenari* image is reproduced with permission.[113] Copyright 2003, The Royal Microscopical Society; the *Aulacoseira valida* image is reproduced with permission.[114] Copyright 2008, Springer; and the *Aulacoseira subarctica* image is Reproduced with permission.[115] Copyright 2008, Springer.

1800940 (16 of 26)

ADVANCED
SCIENCE NEWS
www.advancedsciencenews.com

ADVANCED
MATERIALS
www.advmat.de

to a combination of shear and tensile normal stresses. Anti-trapezoidal interfaces with a bonded tip have the greatest increase in stiffness, strength, and toughness due to the large tip interface area. The insight gained from the mechanical testing of AM-printed suture interfaces is necessary to verify analytical models that can be used to design tailorable geometries for precise mechanical performance.

3.4. Overlapping and Articulated Structures

Overlapping and articulated structures are a hallmark of flexible armor found in fish,[89] reptilian,[90] and mammalian (pangolin[91]) scales. These structured scales enable both flexibility and protection due to the cooperation, in the case of elasmoid fish scales, of a hard-external mineralized phase and a compliant organic tissue. The advent of additive manufacturing has enabled the facile generation of various geometries of articulated and overlapping features to be explored as novel protective systems.

Browning et al.[92] inspired by the overlapping elasmoid scales of the teleost fish, used fused deposition modeling to generate macroscale biomimetic prototypes. ABS was used to mimic the mineralized component and then embedded in silicone rubber to replicate the tissue structure, as shown in **Figure 18**. Three regions are represented in the map of the scale overlap to give angle θ (Figure 18a) that the scales make with the surface (Figure 18b–d). A number of geometric configurations were used adjusting the overlap distance and scale angle to construct a unit with 2–6 repeating scales. The geometric configuration includes aspect ratio, scale orientation angle, spatial overlap, and volume fraction of scales. Plane-strain compression testing was performed to calculate stress, and digital image correlation was used to calculate strain; these values were then compared to a finite element micromechanical model. It was shown that the overlapping scales resist penetration impact by distributing stresses across a large volume, and the flexibility permits rotation and bending under applied loading.[92] The simulations enable verification of the deformation mechanisms and were able to distinguish scale bending, tissue shear, and scale rotations, which were all found to be dependent on the scale geometry. The information gained from the AM-printed prototypes provides the necessary prediction of failure mechanisms in periodic scale assemblies.

Square cross-sectional architectures are not as prominent in nature when compared to

circular cross sections, which makes the seahorse's square tail so peculiar. Porter et al.[93] answered the biological question of "why the articulated bony plates of the seahorse tail are square and not circular" through mechanical testing of 3D-printed prototypes. The structure of the seahorse tail comprises square-articulated plates surrounding the vertebrae as shown in **Figure 19**A. Figure 19B shows simplified CAD assemblies of both square and circular cross sections. PolyJet printing was used to engineer a bioinspired prototype mimicking the square cross-section and compared to a hypothetical circular-cross section prototype. Compression testing was performed on both square and circular prototypes, revealing that the square cross-section withstands higher compressive forces than the cylindrical counterpart (**Figure 20**). Additionally, the square cross-section has a higher rotational stiffness and contact area
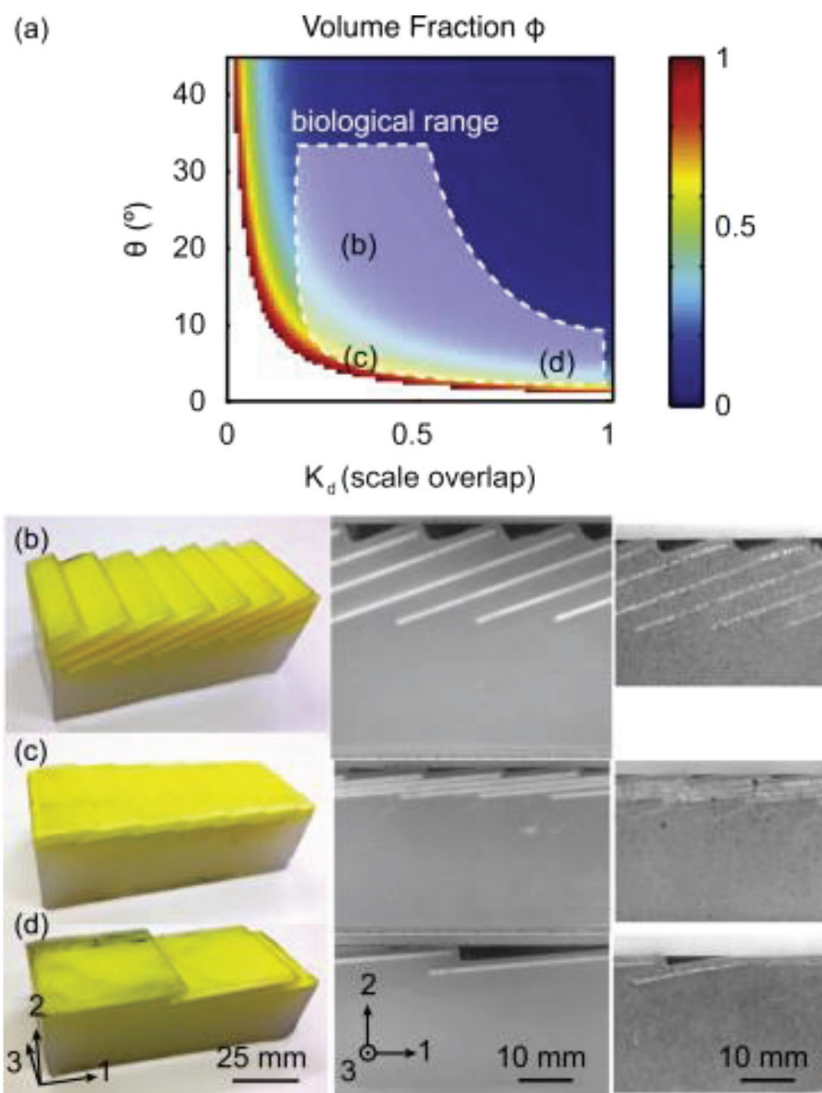
Figure 18. Overlapping bioinspired scales derived from the elasmoid scales of the teleost fish. a) Scale volume fraction φ map. b–d) 3D-printed and molded synthetic scale assembly composed of ABS (yellow) and silicone rubber (translucent) and images from digital image correlation camera prior to loading (center) and deformed (right) for geometries: b) $K_d = 0.3$, $\theta = 20°$, $\varphi = 0.21$, c) $K_d = 0.3$, $\theta = 5°$, $\varphi = 0.77$, and d) $K_d = 0.9$, $\theta = 5°$, $\varphi = 0.26$. Reproduced with permission.[92] Copyright 2013, Elsevier.

**ADVANCED
SCIENCE NEWS**
www.advancedsciencenews.com

**ADVANCED
MATERIALS**
www.advmat.de
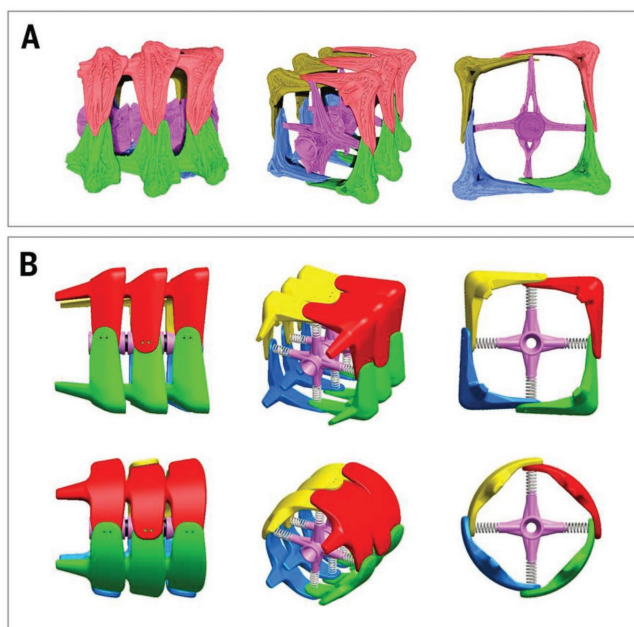
Figure 19. Comparison of µCT images and CAD models of the three segments found in the square seahorse tail and hypothetical circular cross section. a) µCT images of a seahorse tail skeleton (*Hippocampus kuda*). b) CAD models of the square prism (top) and cylindrical (bottom) for 3D-printed prototypes. The color scheme corresponds to the following: vertebrae are color-masked magenta, and the plates are color-masked yellow, red, green, and blue. Reproduced with permission.[93] Copyright 2015, American Association for the Advancement of Science.

than a circular section, ensuring more efficient grasping during prehension of the tail. This is ecologically significant as the seahorse spends most of its life anchored to swaying seaweed. With the use of 3D-printed prototypes, the advantages of the
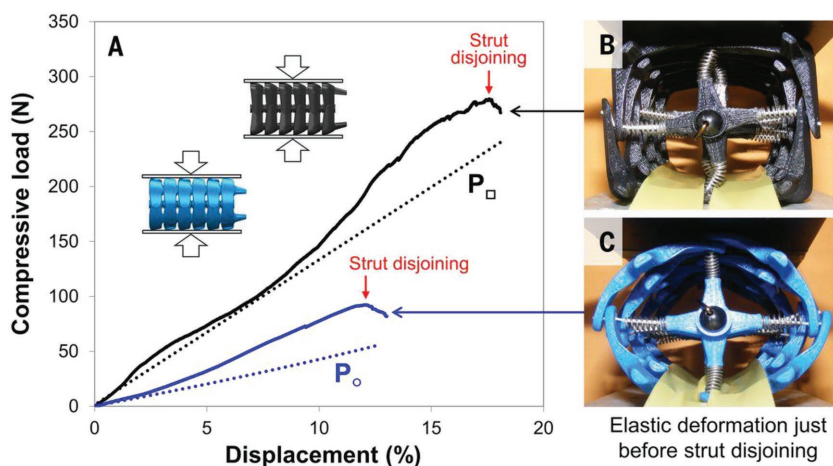
Figure 20. Unilateral compression of the square and cylindrical 3D-printed prototypes inspired by the seahorse tail. A) Plot of the compressive load versus normalized displacement for the square (black) and cylindrical (blue) prototypes. Prototypes were placed between two rigid plates during compression. The solid lines correspond to experimental measurements, while the dashed lines correspond to theoretical predictions. B) Image of the square prototype during unilateral compression just before strut disjoining, corresponding to the red arrows in (A). C) Image of the cylindrical prototype during unilateral compression. Reproduced with permission.[93] Copyright 2015, American Association for the Advancement of Science.

articulated square cross-section were made obvious with benefits in compression, torsion, and prehension.

3.5. Cellular Structures

Cellular structures are inherently lightweight owing to high-porosity architectures. This motif enables directed stress distribution and enhanced energy absorption, which results in the maximum weight–stiffness–strength ratio.[12] This corresponds to materials that increase strength and stiffness while decreasing weight. These structures are advantageous in the biological realm, as it is desirable to expend as little energy and material as possible with the use of a lightweight structure while maintaining strength and stiffness, as demonstrated in the feather vane,[94] cancellous bone,[95] plant stems,[96] and the porcupine quill.[97]

Inspired by the mechanical performance and lightweight structure of balsa wood, Compton and Lewis[46] used direct ink writing to fabricate lightweight-reinforced cellular composites. This technique relies heavily on the use of viscoelastic inks that undergo shear thinning upon extrusion to preferentially align reinforced fibers with thermal curing at elevated temperatures.[46] SiC/C-filled epoxy structures were built with various geometries consisting of square, hexagonal, and triangular honeycomb configuration, with aligned carbon fibers in the print direction, as shown in **Figure 21**. In-plane compression testing was performed to obtain strength values and to deduce failure modes. These structures outperformed commercial 3D-printed structures with Young's modulus of 10–20 times higher. In fact, the Young's modulus was near to those reported for cellular wood, which is quite impressive, despite dissimilarities between bulk cellulose and SiC/C-filled epoxy. Observed failure modes under compression include elastic wall buckling, node rotation, and tensile failure of the cell walls.[46] The enhancement in strength uncovered here is due to the alignment of reinforced carbon fibers made possible by the unique extrusion printing method. This study highlights the importance of design in tailoring strength and damage tolerance of bioinspired materials.

3.6. Bouligand/Helical Structures

Bouligand/helical structures are found in arthropods, where they are composed of layers of chitin fibers forming, by their aggregation, a helical pattern (**Figure 22**).[98] They are also present in fish scales,[99] where the fibers are collagen. A third example is bone osteon,[100] composed of concentric layers of hydroxyapatite/collagen arranged at varying angles to the longitudinal axis. Bouligand/helical structures provide two unique responses for biological materials. First, biological fibers have high tensile strength, but readily flex and buckle under

**ADVANCED
SCIENCE NEWS**
www.advancedsciencenews.com

**ADVANCED
MATERIALS**
www.advmat.de
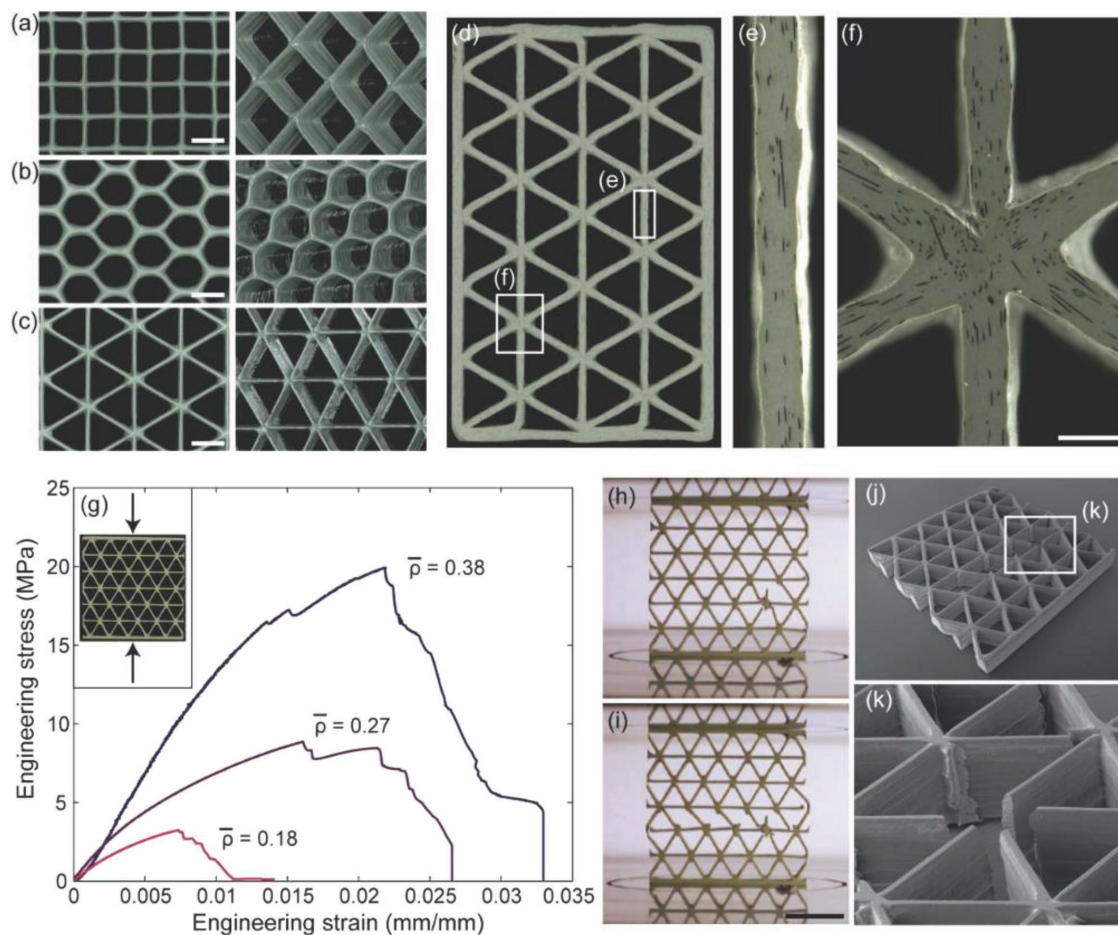
Figure 21. AM of SiC/C-filled epoxy structures with various geometries. a) Square, b) hexagonal, and c) triangular honeycomb structures. Scale bars are 2 mm. d–f) A sequence of optical images of the triangular honeycomb structure. This illustrates that the carbon fibers are highly aligned and oriented along the print direction. The scale bars in (e) and (f) are 500 μm. g) Three compressive stress–strain curves for triangular honeycomb structures with different relative densities. h) Failure mechanisms observed during compression with an initial rotation of a node. f) This is followed by damage propagation, from the site, in the form of elastic wall buckling and tensile fracture. The scale bars for (h) and (i) are 10 mm. j) SEM images of the failure site show an imperfection in the cell wall. This is believed to have influenced the initial node rotation. k) Further magnification of the failure site to recognize the imperfection. Reproduced with permission.[46] Copyright 2015, Wiley-VCH.

compression. By arranging the fibers in a helicoidal fashion, in-plane isotropy of properties can be obtained, together with improved strength in the in-plane direction. Secondly, fracture propagation, which follows an interfiber path, cannot occur in one plane, and is forced to obey the orientation stacking in the Bouligand solid. Thus, the path follows a helical pattern.

This response has been further understood using AM structures, which has demonstrated that the tortuous crack path enhances toughness. Inspired by the dactyl club of the mantis shrimp,[101] which has the ability to deliver blows at an acceleration of $10 \times g$ (terminal velocity of ≈ 2 m s^{-1}), Suksang-panya et al.[102] performed fracture experiments on 3D-printed helicoidal composites. 3D printed prototypes consisting of 28 layers with variations in fiber orientation with ($\gamma = 0°$, 5°, 10°, 30°, and 45°) were printed using the Objet350 Connex PolyJet multimaterial printer (Stratasys Ltd.). The constant pitch angle is denoted by γ and is the angle difference between fiber orientations of adjacent layers. Three-point bending tests

were performed on prenotched samples revealing three competing damage mechanisms. For samples with small γ, the predominant failure mechanism was crack twisting as shown in **Figure 23**. Samples with large γ catastrophically failed by delamination. Secondary crack branching was also observed as a subsidiary mechanism. This study presents guidelines for tailorable damage-tolerant designs using the Bouligand/helical architecture.

3.7. Shape-Morphing Materials

Many biological materials, especially those belonging to plants, have evolved to have a kinetic response to external stimuli. Plants exhibit hydration-induced changes in their morphology due to differences in swelling behavior that originate from the directional orientation of fibers. Examples found in nature are pine cones[103] and seed capsules.[104] Often, the
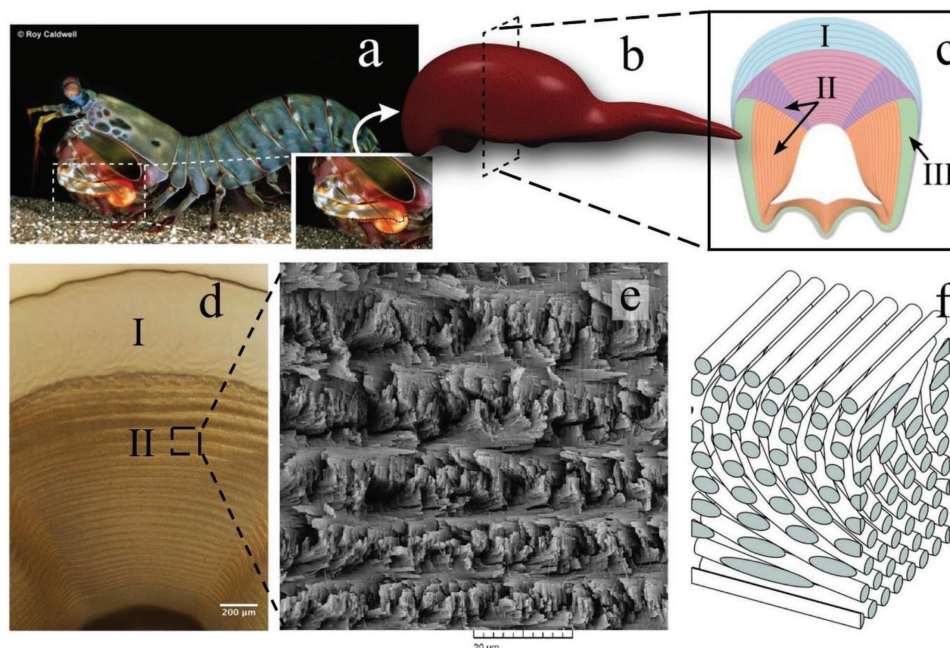
Figure 22. Bouligand structure found in the dactyl club of the mantis shrimp. a) Photograph of the brightly colored mantis shrimp (*Odontodactylus scyllarus*). b) Model of the dactyl club reconstructed from a CT-scanning image. c) Schematic image of a transverse section of the dactyl club highlighting the impact region (I) in blue, the periodic region (II) in pink, purple, and orange, and the striated region (III) in green. d) Optical microscopy image of polished regions I and II. e) SEM image of the fractured surface of the periodic region. f) 3D illustration of Bouligand/helical structure found in the dactyl club. Adapted with permission.[98] Copyright 2015, Elsevier, wherein (a) is adapted with permission.[101] Copyright 2005, The Company of Biologists Ltd. and (e) is adapted with permission.[116] Copyright 2014. Elsevier.

internal structures of plants have a gradient of properties so that swelling takes place preferentially in locations that lead to rotation of the components. Bioinspired materials often rely on a swellable hydrogel composite to achieve an autonomous response. 4D-printing techniques use a hydrogel composite to additively manufacture biomimetic structures.

Gladman et al.[67] inspired by the tissue conformation of shape-morphing plants, used 4D printing to generate composite hydrogel architectures that are encoded with localized, anisotropic swelling, due to the alignment of cellulose fibrils. Target shapes can be programmed to change based on hydration due to the orientation and alignment of stiff cellulose fibers in a hydrogel matrix. This technique enabled the manufacture of complex flower morphologies with a range of shape changing, which was induced by hydration, that rely on geometrical controls.[67] **Figure 24** shows bioinspired flowers constructed using bilayers with different orientations. The layers swell in response to wetting. Differential swelling leads to shape change, which can be tailored by the layering. Figure 24 shows a simple flower shape, whereas the bioinspired orchid (Figure 24e) undergoes shape change that mimics the real *Dendrobium helix* orchid (Figure 24f).

3.8. Structured Surfaces

Nature has evolved specialized surface configurations to perform a diverse range of functions. One of the most spectacular elements is reversible dry adhesion. Adhesion is accomplished through increased van der Waals interactions of nanofibers on the contact surface. This increase in van der Waals forces is propitiated by having increasingly smaller attachment extremities and by correspondingly increasing their number per unit area. Recently, with the use of AM, the geometrical effects of the nanofibers on adhesion has been explored and are being used with potential industrial applications. Using two-photon lithography (Nanoscribe), molds of funnel-shaped microstructures were fabricated to give shape to poly(ethylene glycol) dimethacrylate patterned surfaces with variations in diameter, flap thickness, and the opening angle of the structure, as shown in **Figure 25**.[105] Funnel-shaped microstructures combine the advantages of both mushroom-shaped[106] tips and concave[107] tips. Tailoring the geometry of the fibril tip enables the optimization of the distribution of interfacial stresses. Adhesion testing was performed and results indicate that the funnel-shaped microstructure outperforms other reported structures.[105] This increase in pull-off stresses is attributed to the increase in compliance of the flexible flaps that accommodate surface irregularities and the optimization of interfacial stress distribution.[105] This study highlights the importance of fine-tuning of geometrical features using AM to gain insight from bioinspired microstructures for applications such as dry adhesion.

4. Current Challenges and Future Development

While AM has taken great strides in the past decade to prove itself useful in the development of bioinspired structures, there are still challenges that need to be overcome. A major concern
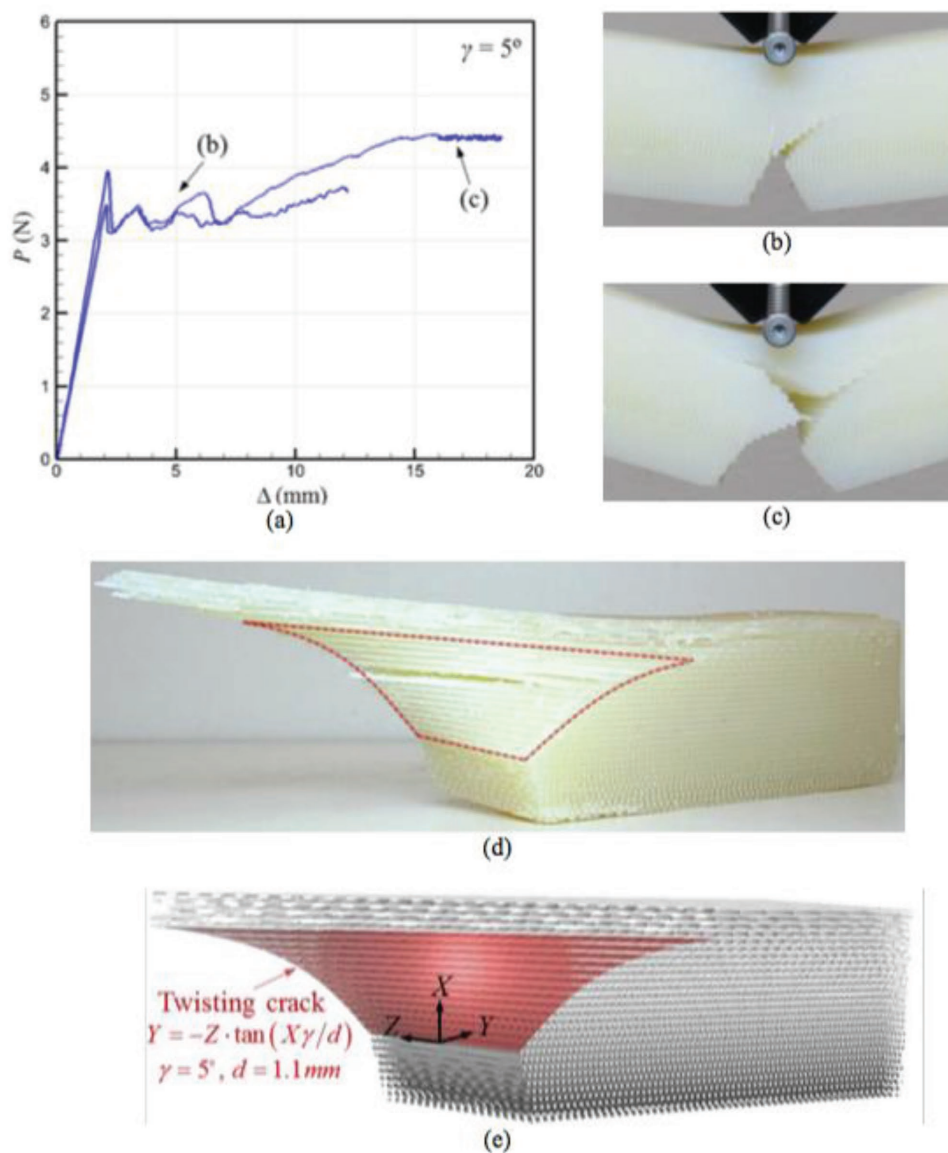
Figure 23. Three-point bending results of 3D-printed helicoidal composite beams with $\gamma = 5°$ inspired by the mantis shrimp. The constant pitch angle is denoted by γ and is the angle difference between fiber orientations of adjacent layers. a) P–Δ plots. b) 5° sample at $\Delta = 5$ mm showing the predominant crack twisting deformation. c) 5° sample at $\Delta = 17$ mm showing extensive crack branching as an additional deformation mechanism. d) The twisting crack surface shown in a cut structure. e) CAD model of 5° sample used to map the crack from fibers at the surface which is characterized by the twisting crack shown as the red surface. Reproduced with permission.[102] Copyright 2018, Elsevier.

is the inherent tradeoff between resolution, build volume, speed, and cost. For amplified resolutions and increased build volume, the speed generally decreases, which in turn increases the cost of production. The following represent the most prevalent challenges:

- *Multiscale*: The remarkable properties of biological materials are predominantly attributed to the organization of design from the nano- to macroscale, which enables the combination of different toughening mechanisms along multiple length scales.[4,69] While commercial AM has the widest range of multiscalability when compared to other traditional methods[108] (due to the diversity of printers and

their resolutions), there does not exist a method to print continuously from nano to macro dimensions. Two-photon polymerization can reach resolutions in the nanoscale with an upper bound of ≈1 µm.[58] On the other hand, many techniques (direct ink writing, photocurable inkjet, and stereolithography) can readily produce complex geometries with micrometer dimensions, but fail to achieve minimum features less than ≈1 µm. True bioinspired constructs necessitate the control of material composition and structure from across great length scales which requires advancements in AM.

- *Multimaterial Interfaces*: Multimaterial printing enables the comparable representation of biological composites; however, uncontrollable mixing occurs at the interface which
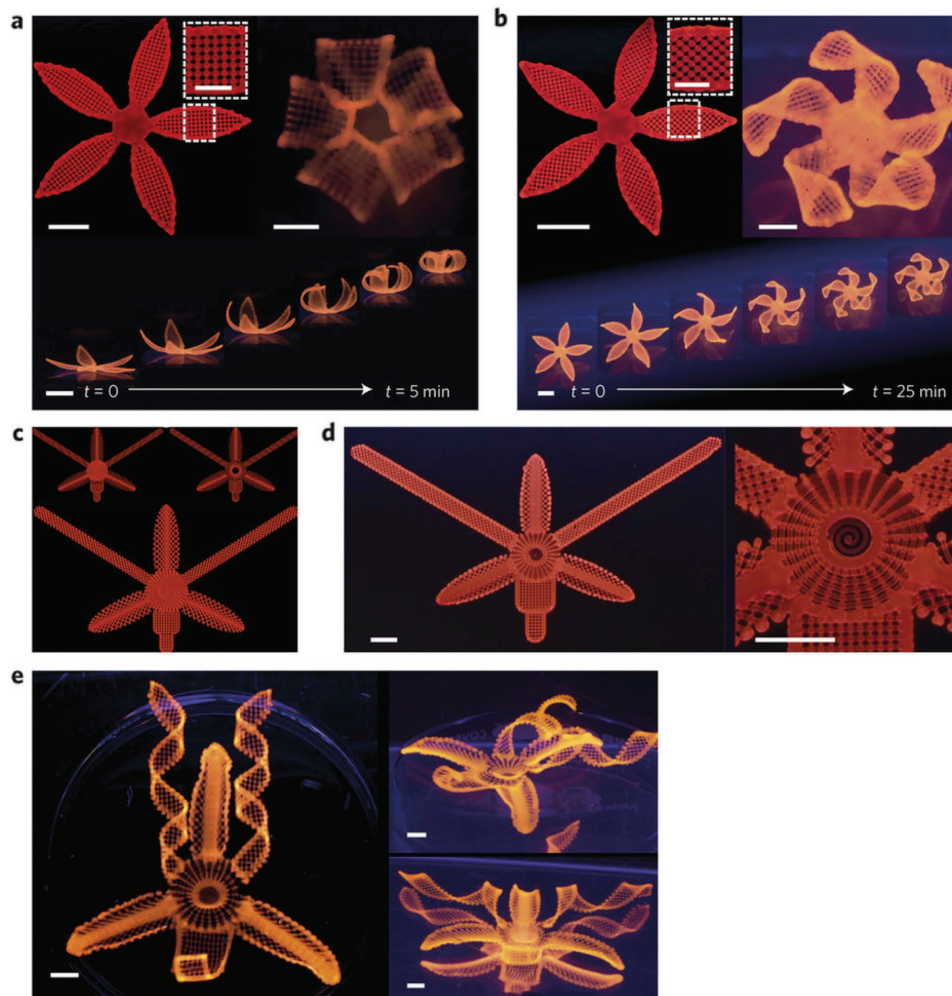
Figure 24. Shape-morphing bioinspired prototypes inspired by intricate flower geometries. a) Simple flowers composed of fibers oriented perpendicular to each other (90°/0°), accompanied by a time-lapse sequence to demonstrate change in shape over 5 min. b) Fibers orientated at angles −45°/45 with a comparable time lapse demonstrating a different closing structure than (a) due to fiber orientation (scale bars, 5 mm; inset = 2.5 mm). c,d) Printed structure detailing fiber orientation. e) Upon swelling, the structure changes shape via twisting, bending, or ruffling dependent on programed fiber orientations. e) An orchid (*D. helix*) demonstrating a range of morphologies found in nature. Reproduced with permission.[67] Copyright 2015, Springer Nature.

leads to unpredictable properties.[15] This topic is currently being explored and it is understood that the combinations of different materials, load directions, and mixing ratios all contribute to variations in interfacial properties with multiple consequences.[109] There exists a threshold above which the "composite effect" (when the size of the feature is 2 orders of magnitude larger than the inclusion size)[109] needs to be taken into account. The interfacial properties of multimaterial printing need to be fully investigated to better control and tailor bioinspired prototypes.

- *Inherent Defect Control*: Additive manufacturing systems are known to produce prototypes with minor defects due to their inability to detect and correct errors during production.[110] These compounding errors often lead to voids and inconsistent prototypes. This is inherently detrimental to studying bioinspired designs, as structure and geometry play key roles in property determination. A proposed solution to quality assessment is the use of software imaging analysis.[110]

This solution enables the detection of defects where the filament has not been applied. While this technique only detects limited defects, it will be necessary to develop more robust solutions that can identify and correct a range of defects. It is important to note that defects are inherent in biological materials and can contribute to toughening and strengthening. These defects arise from the fact that most biological materials are multifunctional, which have channels or pores creating structural voids or empty spaces in the material. For example, the pores in bone tissue direct a load from weak to strong areas. AM does not have to produce perfect architectures, but when performing a systematic study of various geometries on crack propagation, the introduction of unwanted defects can introduce unintended and disruptive features as seen in the study by Dimas et al.[71]

For the future direction of the field of biological materials and AM, it will be important to increase functionality of fabricated

ADVANCED
SCIENCE NEWS

www.advancedsciencenews.com

ADVANCED
MATERIALS

www.advmat.de
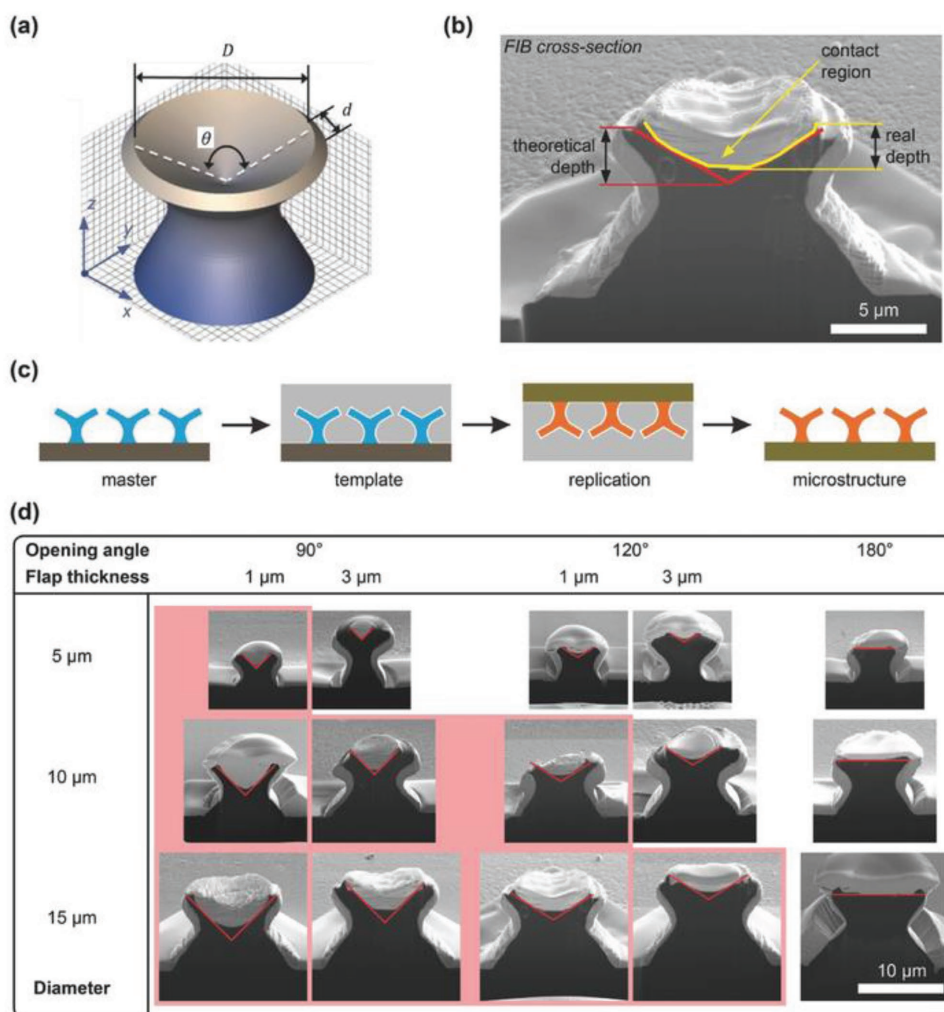
Figure 25. Illustration and comparison of variation in opening angle and flap thickness of funnel-shaped microstructures inspired by the structured surfaces of the gecko pad. a) CAD model for printing using two-photon lithography. The diameter, D, the flap thickness, d, and the opening angle, θ, of the funnels vary across different samples. b) SEM image of an FIB cross-section (D = 15 μm, d = 1 μm, θ = 120°) funnel-shaped microstructure. Variations between real structures (yellow contour line) and the intended CAD models (red contour line) are predominantly due to material shrinkage. c) Schematic of the manufacturing process of funnel-shaped PEGdma structures. Beginning with the master structures (blue), which were fabricated using two-photon lithography on a glass substrate and were subsequently replicated onto PDMS (grey). This template was in turn used to fabricate the funnel-shaped structures out of PEGdma (orange). d) Secondary electron images of FIB cross-sections of various funnel-shaped microstructures with differences in flap thickness and angle. The structures highlighted in red exhibit pull-off stresses higher than 1 MPa. Reproduced with permission.[105] Copyright 2017, Wiley-VCH.

components with the use of multiprocess 3D printing. Multiprocess 3D printing combines complementary processes to potentially include electronic, electromagnetic, optical, chemical, and thermal features.[111] Biological materials are known for their multifunctional capabilities[12]; for example, fish scales[112] can provide camouflage, mechanical protection, flexibility, and low water drag. A fundamental understanding of these systems can be applied to bioinspired material designs. To do so, it will become necessary to use multiprocess 3D printing. Additionally, the patterns and structures reported here are far removed from the complexity found in nature. While the goal of this work is not to exactly reproduce what nature has accomplished, the next stage is to match a more similar degree of complexity that will lead to fine-tuned features and properties necessary to develop novel synthetic materials. This will require advances in

resolution and multiscalability. Additive manufacturing's growth projection is dynamic and rapidly improving, which gives unlimited potential for future work in bioinspired design and integration.

While there are considerable advancements that need to occur in AM technology to enhance the field of bioinspired materials, it is also important to improve our understanding of the fundamental behavior of biological materials. As we develop superior characterization and analytical techniques, such as in situ cryoelectron microscopy, we can reveal with more accuracy the molecular assemblies of chemically unmodified specimens. Biological materials are a part of living systems, and, therefore, it is important to study them in an unaltered state. Another important consideration is understanding how the overall mechanical behavior of the material influences the governing

Table 1. A summary of the properties and mechanisms explored with each bioinspired structure and the corresponding AM technique used.

Properties/mechanisms explored	Bioinspired structure/features	AM method
Damping/energy dissipation	- Volume fraction of stiff material in layered composites inspired by bone and nacre - Topology of bone inspired layered composites - Architectural features of mineral bridges in layered composites	PolyJet (Stratasys Ltd.)
Fracture toughness/strength	- Brick morphology in brick-and-mortar like structures	Fused deposition modeling
Damage tolerant hierarchies	- Hierarchical nanolattices inspired by the length scales in many biological materials - Cross-lamellar hierarchies for crack deflection inspired by nacre	Two-photon polymerization (Nanoscribe) and PolyJet (Stratasys Ltd.)
Stiffness and strength	- Jigsaw-like sutures inspired by diatoms - Sutures with trapezoidal interlocking features inspired by diatoms	Digital light processing technology (Micro HiRes Machine, Envision Tech), PolyJet (Stratasys Ltd.)
Flexible and damage tolerant	- Geometries of overlapping scales inspired by elasmoid fish scales - Comparison between square and circular cross-sectional architectures of articulated scales inspired by the seahorse tail	PolyJet (Stratasys Ltd.), fused deposition modeling
Stiffness, strength, and lightweight structures	- Geometry of foam architectures	Direct ink printing
Damage mechanisms in Bouligand/helical structures	- Variations in fiber orientation angles in Bouligand structures	PolyJet (Stratasys Ltd.)
Shape morphing	- Orientation of fibers in a hydrogel matrix inspired by the dynamic movement of plants	4D printing
Dry adhesion	- Geometrical effects of the tip of nanofibers inspired by gecko adhesion	Two-photon polymerization (Nanoscribe)

mechanisms, which we may not be able to capture when only looking at a particular length scale. To drive the field of bioinspired materials forward, we need to obtain a more holistic understanding of biological materials, which comes with better hypothesis and advancements in the technological tools to unearth what is unknown.

5. Conclusions

Additive manufacturing is becoming an integral part of research on biological and bioinspired materials as clearly demonstrated here. It provides the capabilities to generate intricate designs needed to investigate geometrical effects on mechanical performance in bioinspired structures. AM is a rapidly evolving technique, and while many methods exist for the design and fabrication of bioinspired materials, it is evident that PolyJet multimaterial printing (Stratasys Ltd.) and two-photon polymerization (Nanoscribe) are integral players in this field. Nature's reliance on the integration of both soft and hard materials to achieve exceptional properties makes multimaterial printing a necessity. With the advancement of powerful lasers, two-photon polymerization has emerged with the capability of nanoscale dimensions to generate structures on a fundamental scale that is critical to the success of biological materials.

AM provides a tailorable tool to explore cardinal structural interactions and optimize properties. This phenomenal tool can be used in two primary modes:

- To assist in our understanding of the mechanisms and response to external loads (deformation, damage, and failure).

Specific mechanisms identified in biological materials are incorporated into additive-manufactured designs. These are then manufactured and tested under distinct conditions to identify the mechanisms, test the hypotheses, and improve our understanding. Lessons from nature are translated into designs that use the principles at hand and are tailored to suit a particular application, which may be quite different from the natural system. One example that stands out is the potential industrial application of gecko-inspired dry adhesives.

- Bioinspired designs can be optimized by systematic variations of the material and geometric parameters. Thus, combined with analysis (such as FEA), 3D printing can lead to optimized designs as shown in the process map of Figure 4.

The properties and mechanisms uncovered here, with the use of AM to generate systematic and complex bioinspired structures, are outlined in **Table 1**. This table highlights that a diverse range of properties can be explored using AM.

Acknowledgements

Conflict of Interest

The authors declare no conflict of interest.

Keywords

[1] M. A. Meyers, P.-Y. Chen, A. Y.-M. Lin, Y. Seki, *Prog. Mater. Sci.* **2008**, *53*, 1.
[2] M. A. A. Meyers, J. McKittrick, P.-Y. Y. Chen, *Science* **2013**, *339*, 773.
[3] M. A. Meyers, P.-Y. Chen, M. I. Lopez, Y. Seki, A. Y. M. Lin, *J. Mech. Behav. Biomed. Mater.* **2011**, *4*, 626.
[4] R. O. Ritchie, *MRS Bull.* **2014**, *39*, 880.
[5] E. Arzt, *Mater. Sci. Eng., C* **2006**, *26*, 1245.
[6] P. Y. Chen, J. McKittrick, M. A. A. Meyers, *Prog. Mater. Sci.* **2012**, *57*, 1492.
[7] S. Zhang, *Mater. Today* **2003**, *6*, 20.
[8] P.-Y. Chen, A. Y. M. Lin, Y.-S. Lin, Y. Seki, A. G. Stokes, J. Peyras, E. A. Olevsky, M. A. Meyers, J. McKittrick, *J. Mech. Behav. Biomed. Mater.* **2008**, *1*, 208.
[9] S. Weiner, H. D. Wagner, *Annu. Rev. Mater. Sci.* **1998**, *28*, 271.
[10] J. Y. Rho, L. Kuhn-Spearing, P. Zioupos, *Med. Eng. Phys.* **1998**, *20*, 92.
[11] P. Fratzl, H. S. Gupta, E. P. Paschalis, P. Roschger, *J. Mater. Chem.* **2004**, *14*, 2115.
[12] S. E. Naleway, M. M. Porter, J. McKittrick, M. A. Meyers, *Adv. Mater.* **2015**, *27*, 5455.
[13] M. F. Ashby, L. J. Gibson, U. Wegst, R. Olive, *Proc. R. Soc. London, Ser. A* **1995**, *450*, 123.
[14] H. D. Espinosa, J. E. Rim, F. Barthelat, M. J. Buehler, *Prog. Mater. Sci.* **2009**, *54*, 1059.
[15] W. Gao, Y. Zhang, D. Ramanujan, K. Ramani, Y. Chen, C. B. Williams, C. C. L. Wang, Y. C. Shin, S. Zhang, P. D. Zavattieri, *Comput. Des.* **2015**, *69*, 65.
[16] M. Rühle, A. G. Evans, *Prog. Mater. Sci.* **1989**, *33*, 85.
[17] S. Patra, V. Young, *Cell Biochem. Biophys.* **2016**, *74*, 93.
[18] J. An, J. E. M. Teoh, R. Suntornnond, C. K. Chua, *Engineering* **2015**, *1*, 261.
[19] H. N. Chia, B. M. Wu, *J. Biol. Eng.* **2015**, *9*, 4.
[20] J. Malda, J. Visser, F. P. Melchels, T. Jüngst, W. E. Hennink, W. J. A. Dhert, J. Groll, D. W. Hutmacher, *Adv. Mater.* **2013**, *25*, 5011.
[21] B. Derby, *Science* **2012**, *338*, 921.
[22] G. Villar, A. D. Graham, H. Bayley, *Science* **2013**, *340*, 48.
[23] S. V. Murphy, A. Atala, *Nat. Biotechnol.* **2014**, *32*, 773.
[24] M. Guvendiren, J. Molde, R. M. D. Soares, J. Kohn, *ACS Biomater. Sci. Eng.* **2016**, *2*, 1679.
[25] C. L. Ventola, *Pharm. Ther.* **2014**, *39*, 704.
[26] A. A. Giannopoulos, D. Mitsouras, S.-J. Yoo, P. P. Liu, Y. S. Chatzizisis, F. J. Rybicki, *Nat. Rev. Cardiol.* **2016**, *13*, 701.
[27] R. J. Morrison, S. J. Hollister, M. F. Niedner, M. G. Mahani, A. H. Park, D. K. Mehta, R. G. Ohye, G. E. Green, *Sci. Transl. Med.* **2015**, *7*, 285ra64.
[28] M. K. Gupta, F. Meng, B. N. Johnson, Y. L. Kong, L. Tian, Y. W. Yeh, N. Masters, S. Singamaneni, M. C. McAlpine, *Nano Lett.* **2015**, *15*, 5321.
[29] C. Ortiz, M. C. Boyce, *Science* **2008**, *319*, 1053.
[30] Q. Wang, Q. Meng, P. Wang, H. Liu, L. Jiang, *ACS Nano* **2015**, *9*, 4362.
[31] A. R. Studart, *Chem. Soc. Rev.* **2016**, *45*, 359.
[32] C. Zhang, D. A. Mcadams, J. C. Grunlan, *Adv. Mater.* **2016**, *28*, 8566.
[33] A. A. Zadpoor, J. Malda, *Ann. Biomed. Eng.* **2017**, *45*, 1.
[34] G. X. Gu, I. Su, S. Sharma, J. L. Voros, Z. Qin, M. J. Buehler, *J. Biomech. Eng.* **2016**, *138*, 021006.
[35] H.-B. Yao, H.-Y. Fang, X.-H. Wang, S.-H. Yu, *Chem. Soc. Rev.* **2011**, *40*, 3764.
[36] B. Derby, *Annu. Rev. Mater. Res.* **2010**, *40*, 395.
[37] J. A. Lewis, *Adv. Funct. Mater.* **2006**, *16*, 2193.
[38] T. Köpplmayr, M. Mühlberger, *J. Appl. Polym. Sci.* **2016**, *133*, 43527.
[39] R. A. Barry, R. F. Shepherd, J. N. Hanson, R. G. Nuzzo, P. Wiltzius, J. A. Lewis, *Adv. Mater.* **2009**, *21*, 2407.
[40] D. S. Ginger, H. Zhang, C. A. Mirkin, *Angew. Chem., Int. Ed.* **2004**, *43*, 30.
[41] J. E. Smay, J. Cesarano, J. A. Lewis, *Langmuir* **2002**, *18*, 5429.
[42] G. M. Gratson, J. A. Lewis, *Langmuir* **2005**, *21*, 457.
[43] B. Y. Ahn, E. B. Duoss, M. J. Motala, X. Guo, S. Il Park, Y. Xiong, J. Yoon, R. G. Nuzzo, J. A. Rogers, J. A. Lewis, *Science* **2009**, *323*, 1590.
[44] C. J. Ferris, K. G. Gilmore, G. G. Wallace, M. In Het Panhuis, *Appl. Microbiol. Biotechnol.* **2013**, *97*, 4243.
[45] T. A. Campbell, O. S. Ivanova, *Nano Today* **2013**, *8*, 119.
[46] B. G. Compton, J. A. Lewis, *Adv. Mater.* **2014**, *26*, 5930.
[47] F. P. W. Melchels, J. Feijen, D. W. Grijpma, *Biomaterials* **2010**, *31*, 6121.
[48] C. M. Yakacki, R. Shandas, C. Lanning, B. Rech, A. Eckstein, K. Gall, *Biomaterials* **2007**, *28*, 2255.
[49] J. J. Martin, B. E. Fiore, R. M. Erb, *Nat. Commun.* **2015**, *6*, 8641.
[50] S. Kumar, M. Hofmann, B. Steinmann, E. J. Foster, C. Weder, *ACS Appl. Mater. Interfaces* **2012**, *4*, 5399.
[51] M. R. Sommer, R. M. Erb, A. R. Studart, *ACS Appl. Mater. Interfaces* **2012**, *4*, 5086.
[52] F. P. W. Melchels, K. Bertoldi, R. Gabbrielli, A. H. Velders, J. Feijen, D. W. Grijpma, *Biomaterials* **2010**, *31*, 6909.
[53] F. P. W. Melchels, M. A. N. Domingos, T. J. Klein, J. Malda, P. J. Bartolo, D. W. Hutmacher, *Prog. Polym. Sci.* **2012**, *37*, 1079.
[54] J. R. C. Dizon, A. H. Espera, Q. Chen, R. C. Advincula, *Addit. Manuf.* **2018**, *20*, 44.
[55] R. L. Truby, J. A. Lewis, *Nature* **2016**, *540*, 371.
[56] M. W. Barclift, C. B. Williams, in *Proc. Solid Freeform Fabrication Symposium*, Defense Technical Information Center, Fort Belvoir, VA, USA **2012**, pp. 876–890.
[57] B. N. Chichkov, A. Ostendorf, *Photonics Spectra* **2006**, *40*, 72.
[58] L. L. Erskine, A. A. Heikal, S. M. Kuebler, M. Rumi, X. Wu, S. R. Marder, J. W. Perry, *Solid State Phys.* **1999**, *398*, 51.
[59] U. G. K. Wegst, H. Bai, E. Saiz, A. P. Tomsia, R. O. Ritchie, C. Ortiz, M. Boyce, U. G. K. Wegst, H. Bai, E. Saiz, A. P. Tomsia, R. O. Ritchie, *Nat. Mater.* **2014**, *14*, 23.
[60] H. Le Ferrand, F. Bouville, T. P. Niebel, A. R. Studart, *Nat. Mater.* **2015**, *14*, 1172.
[61] R. M. Erb, R. Libanori, N. Rothfuchs, A. R. Studart, *Science* **2012**, *335*, 199.
[62] F. Momeni, S. M. Mehdi Hassani, N. X. Liu, J. Ni, *Mater. Des.* **2017**, *122*, 42.
[63] Q. Ge, H. J. Qi, M. L. Dunn, *Appl. Phys. Lett.* **2013**, *103*, 131901.
[64] B. Gao, Q. Yang, X. Zhao, G. Jin, Y. Ma, F. Xu, *Trends Biotechnol.* **2016**, *34*, 746.
[65] Y. C. Li, Y. S. Zhang, A. Akpek, S. R. Shin, A. Khademhosseini, *Biofabrication* **2016**, *9*, 012001.
[66] S. K. Leist, J. Zhou, *Virtual Phys. Prototyping* **2016**, *11*, 249.

[67] A. Sydney Gladman, E. A. Matsumoto, R. G. Nuzzo, L. Mahadevan, J. A. Lewis, *Nat. Mater.* **2016**, *15*, 413.

[68] P. Zhang, M. A. Heyne, A. C. To, *J. Mech. Phys. Solids* **2015**, *83*, 285.

[69] R. O. Ritchie, *Nat. Mater.* **2011**, *10*, 817.

[70] M. Sarikaya, K. E. Gunnison, M. Yasrebi, I. A. Aksay, *Mater. Reseaerch Soc. Symp.* **1990**, *174*, 109.

[71] L. S. Dimas, G. H. Bratzel, I. Eylon, M. J. Buehler, *Adv. Funct. Mater.* **2013**, *23*, 4629.

[72] J. D. Currey, J. D. Taylor, *J. Zool.* **1974**, *173*, 395.

[73] G. X. Gu, F. Libonati, S. D. Wettermark, M. J. Buehler, *J. Mech. Behav. Biomed. Mater.* **2017**, *76*, 135.

[74] F. Barthelat, R. Rabiei, *J. Mech. Phys. Solids* **2011**, *59*, 829.

[75] H. D. Espinosa, A. L. Juster, F. J. Latourte, O. Y. Loh, D. Gregoire, P. D. Zavattieri, *Nat. Commun.* **2011**, *2*, 173.

[76] J. E. Rim, P. Zavattieri, A. Juster, H. D. Espinosa, *J. Mech. Behav. Biomed. Mater.* **2011**, *4*, 190.

[77] L. R. Meza, A. J. Zelhofer, N. Clarke, A. J. Mateos, D. M. Kochmann, J. R. Greer, *Proc. Natl. Acad. Sci. USA* **2015**, *112*, 11502.

[78] P. Fratzl, R. Weinkamer, *Prog. Mater. Sci.* **2007**, *52*, 1263.

[79] J. Aizenberg, J. C. Weaver, M. S. Thanawala, V. C. Sundar, D. E. Morse, P. Fratzl, *Science* **2005**, *309*, 275.

[80] G. X. Gu, M. Takaffoli, M. J. Buehler, *Adv. Mater.* **2017**, *29*, 1.

[81] R. Menig, M. H. Meyers, M. A. Meyers, K. S. Vecchio, *Mater. Sci. Eng., A* **2001**, *297*, 203.

[82] W. Yang, S. E. Naleway, M. M. Porter, M. A. Meyers, J. McKittrick, *Acta Biomater.* **2015**, *23*, 1.

[83] Z. Sun, E. Lee, S. W. Herring, *Anat. Rec.* **2004**, *276A*, 150.

[84] I. H. Chen, W. Yang, M. A. Meyers, *Acta Biomater.* **2015**, *28*, 2.

[85] B. Achrai, H. Daniel Wagner, *Mater. Sci. Eng., C* **2015**, *53*, 128.

[86] I. A. A. Malik, M. Mirkhalaf, F. Barthelat, *J. Mech. Phys. Solids* **2017**, *102*, 224.

[87] E. Lin, Y. Li, C. Ortiz, M. C. Boyce, *J. Mech. Phys. Solids* **2014**, *73*, 166.

[88] M. De Stefano, L. De Stefano, R. Congestri, *Superlattices Microstruct.* **2009**, *46*, 64.

[89] W. Yang, B. Gludovatz, E. A. Zimmermann, H. A. Bale, R. O. Ritchie, M. A. Meyers, *Acta Biomater.* **2013**, *9*, 5876.

[90] D. L. Hu, J. Nirody, T. Scott, M. J. Shelley, *Proc. Natl. Acad. Sci. USA* **2009**, *106*, 10081.

[91] B. Wang, W. Yang, V. R. Sherman, M. A. Meyers, *Acta Biomater.* **2016**, *41*, 60.

[92] A. Browning, C. Ortiz, M. C. Boyce, *J. Mech. Behav. Biomed. Mater.* **2013**, *19*, 75.

[93] M. M. Porter, D. Adriaens, R. L. Hatton, M. A. Meyers, J. McKittrick, *Science* **2015**, *349*, aaa6683.

[94] T. N. Sullivan, A. Pissarenko, S. A. Herrera, D. Kisailus, V. A. Lubarda, M. A. Meyers, *Acta Biomater.* **2016**, *41*, 27.

[95] D. R. Carter, W. C. Hayes, *J. Bone Jt. Surg.* **1977**, *59*, 954.

[96] L. J. Gibson, *J. Biomech.* **2005**, *38*, 377.

[97] W. Yang, C. Chao, J. McKittrick, *Acta Biomater.* **2013**, *9*, 5297.

[98] N. Guarín-Zapata, J. Gomez, N. Yaraghi, D. Kisailus, P. D. Zavattieri, *Acta Biomater.* **2015**, *23*, 11.

[99] E. A. Zimmermann, B. Gludovatz, E. Schaible, N. K. N. Dave, W. Yang, M. A. Meyers, R. O. Ritchie, *Nat. Commun.* **2013**, *4*, 2634.

[100] M. M. Giraud-Guille, *Calcif. Tissue Int.* **1988**, *42*, 167.

[101] S. N. Patek, *J. Exp. Biol.* **2005**, *208*, 3655.

[102] N. Suksangpanya, N. A. Yaraghi, R. B. Pipes, D. Kisalius, P. Zavattieri, *Int. J. Solids Struct.* **2018**, https://doi.org/10.1016/j.ijsolstr.2018.06.004.

[103] A. R. Studart, R. M. Erb, *Soft Matter* **2014**, *10*, 1284.

[104] M. J. Harrington, K. Razghandi, F. Ditsch, L. Guiducci, M. Rueggeberg, J. W. C. Dunlop, P. Fratzl, C. Neinhuis, I. Burgert, *Nat. Commun.* **2011**, *2*, 337.

[105] S. C. L. Fischer, K. Groß, O. Torrents Abad, M. M. Becker, E. Park, R. Hensel, E. Arzt, *Adv. Mater. Interfaces* **2017**, *4*, 1700292.

[106] A. Del Campo, C. Greiner, E. Arzt, *Langmuir* **2007**, *23*, 10235.

[107] R. Spolenak, S. Gorb, H. Gao, E. Arzt, *Proc. R. Soc. London, Ser. A* **2005**, *461*, 305.

[108] V. Khare, S. Sonkaria, G. Y. Lee, S. H. Ahn, W. S. Chu, *Int. J. Precis. Eng. Manuf. – Green Technol.* **2017**, *4*, 291.

[109] J. Mueller, D. Courty, M. Spielhofer, R. Spolenak, K. Shea, *3D Print. Addit. Manuf.* **2017**, *4*, 193.

[110] J. Straub, *Machines* **2015**, *3*, 55.

[111] E. MacDonald, R. Wicker, *Science* **2016**, *353*, aaf2093.

[112] Z. Sun, T. Liao, W. Li, Y. Dou, K. Liu, L. Jiang, S. W. Kim, J. H. Kim, S. Xue Dou, *NPG Asia Mater.* **2015**, *7*, e232.

[113] I. C. Gebeshuber, J. H. Kindt, J. B. Thompson, Y. Del Amo, H. Stachelberger, M. A. Brzezinski, G. D. Stucky, D. E. Morse, P. K. Hansma, *J. Microsc.* **2003**, *212*, 292.

[114] G. I. Popovskaya, S. I. Genkal, *Inland Water Biol.* **2008**, *1*, 311.

[115] S. I. Genkal, G. I. Popovskaya, *Inland Water Biol.* **2008**, *1*, 120.

[116] L. K. Grunenfelder, N. Suksangpanya, C. Salinas, G. Milliron, N. Yaraghi, S. Herrera, K. Evans-Lutterodt, S. R. Nutt, P. Zavattieri, D. Kisailus, *Acta Biomater.* **2014**, *10*, 3997.

1800940 (26 of 26)